Universidade de Aveiro
Ano 2012

Departamento de
Engenharia Mecânica

Vienna University of
Technology
Year 2012

Institute of Lightweight
Design and Structural
Biomechanics

ANDREY KHOLKIN

SIMULAÇÃO DE DANO E FRACTURA EM ENSAIOS DE FLEXÃO EM 3 PONTOS EM PROVETES LAMINADOS

NUMERICAL SIMULATION OF DAMAGE AND FAILURE OF LAMINATED 3-POINT BENDING SPECIMENS

Dissertação apresentada à Universidade de Aveiro para cumprimento dos requisitos necessários à obtenção do grau de Mestre em Engenharia Mecânica, realizada sob a orientação científica do Prof. Heinz Pettermann, Professor Associado do "Institute of Lightweight Design and Structural Biomechanics in Vienna University of Technology" e do Dipl. Ing. Jakob Gager, aluno PhD do "Institute of Lightweight Design and Structural Biomechanics in Vienna University of Technology".

Thesis presented to the University of Aveiro to follow the necessary requirements for obtaining the Master degree in Mechanical Engineering, under the supervision of Prof. Heinz Pettermann, Associate Professor of the Institute of Lightweight Design and Structural Biomechanics of the Vienna University of Technology and Dipl. Ing. Jakob Gager, PhD student of the Institute of Lightweight Design and Structural Biomechanics of the Vienna University of Technology.

o júri

presidente Prof. Heinz Pettermann

Professor Associado do “Institute of Lightweight Design and Structural Biomechanics in Vienna University of Technology” (orientador)

Dipl. Ing. Jakob Gager

Aluno PhD do “Institute of Lightweight Design and Structural Biomechanics in Vienna University of Technology” (co-orientador)

Prof. Dr. António Gil d’Orey de Andrade Campos

Professor Auxiliar Convidado da Universidade de Aveiro

agradecimentos

I would like to thank Professor Heinz Pettermann and Dipl. Ing. Jakob Gager for the knowledge, experience, and help they offered to me, and their availability and professionalism. I would also like to thank the rest of the staff from the Institute of Lightweight Design and Structural Biomechanics of the Vienna University of Technology for the positive working environment.

Quero também agradecer aos professores do Departamento de Engenharia Mecânica por me terem dado uma excelente formação na área de engenharia mecânica e aos meus pais por me terem apoiado durante os meus estudos.

palavras-chave

Modelação de dano, laminados, ensaios de flexão em 3 pontos, método dos elementos finitos.

resumo

Polímeros reforçados por fibras (PRF) tem sido utilizados durante muito tempo para aplicações estruturais, particularmente com laminados. No projeto de laminados é importante caracterizar o seu comportamento mecânico.

O comportamento mecânico é caracterizado por uma rigidez inicial e pela fractura. A estratégia de modelação utilizada nesta dissertação permite não só prever o “first-ply-failure”, como também modelar a sequência de eventos a seguir, como a delaminação e a fractura final da estrutura. Para isso é utilizado um modelo para a interface e para as camadas, permitindo a interação entre eles.

A rigidez inicial também é avaliada com diferentes ratios comprimento para espessura, permitindo também diferentes contribuições do cisalhamento transversal e de flexão.

Nesta dissertação com o método dos elementos finitos (FEM) é investigado o comportamento estrutural de uma viga compósita sobe ensaios de flexão em três pontos. Para este fim o programa comercial Abaqus é utilizado, permitindo simulações numéricas com elementos continuum casca e elementos convencionais casca. Também são realizadas simulações numéricas de modo a preparar a resultados para uma futura experiência, para o qual o tamanho do provete é escolhido com recomendações do EN ISO 14125.

keywords

Damage modeling, laminates, 3 point bending simulations, finite element method

abstract

Fiber-reinforced polymers (FRP) have been used for a long time for structural applications, particularly with laminates. It is important to characterize the mechanical behavior of laminates for their design.

This behavior is characterized by an initial stiffness and by failure. The modeling strategy used in this thesis allows to predict not only first-ply-failure (FPF), but also to model the sequence of events afterwards, such as delamination and the final failure of the structure. This is achieved by using a damage model for the ply and for the interface, allowing the interaction between them.

The initial stiffness is also evaluated with different length to thickness ratios, allowing different contributions from transverse shear and bending.

In this thesis, with the finite element method (FEM) the structural behavior of a laminate composite beam under a three point bending configuration is investigated. For this purpose the commercial FEM package Abaqus is used, allowing numerical simulations with continuum shell and conventional shell elements. Also simulations are conducted, in order to prepare a future experiment for which the specimen size was chosen with recommendations from EN ISO 14125.

Content

List of Figures

List of Tables

1. Introduction

1.1. Composite engineering

Composite engineering is widely used in the development of structures that require a higher strength in one direction. The higher strength can be achieved by using fiber reinforced composites (FRC). The matrix is reinforced by short or long fibers oriented in a certain direction, which gives orthotropic behavior for the composite. The fibers can be also randomly disposed in the matrix with no preferential direction, then giving an isotropic behavior. Both fiber and matrix can be metal, ceramic or polymer material. In cases where the matrix is polymer these are called fiber reinforced polymers (FRP).

The fiber has typically high strength and low density, while the matrix can be ductile or brittle. The composite's final compressive and tensile strength and stiffness depend on the fiber volume fraction, type and arrangement. The effective or overall material parameters of the composite are usually obtained through experimental methods. When such data is not available except of constituent parameters, then numerical or analytical micro-mechanical techniques are required.

In most cases composite engineering requires the use of laminates. These consist of several plies or laminae with different orientations connected together through a bonding interface, choosing the correct stacking sequence is important for the overall strength and stiffness of the structure. The combination of a type of matrix and fiber allows for applications not possible with conventional materials, but on the downside they are more expensive, so the design of composites must be chosen based on their cost and should be structurally beneficial, because perpendicular directions are weaker (transverse direction for a single ply and out-of-plane direction for a laminate).

1.2. Composite applications

Metallic structures have been replaced in many applications by composites. The comparison between metals and composites can be found in Figure 1.1 [14]. Specific strength and stiffness are much higher for the unidirectional lamina, but the clear disadvantage is the lack of isotropy. If the in-plane loading is equal in both directions, then a biaxially isotropic laminate can be used, but then the advantage of using composite material is not so pronounced.

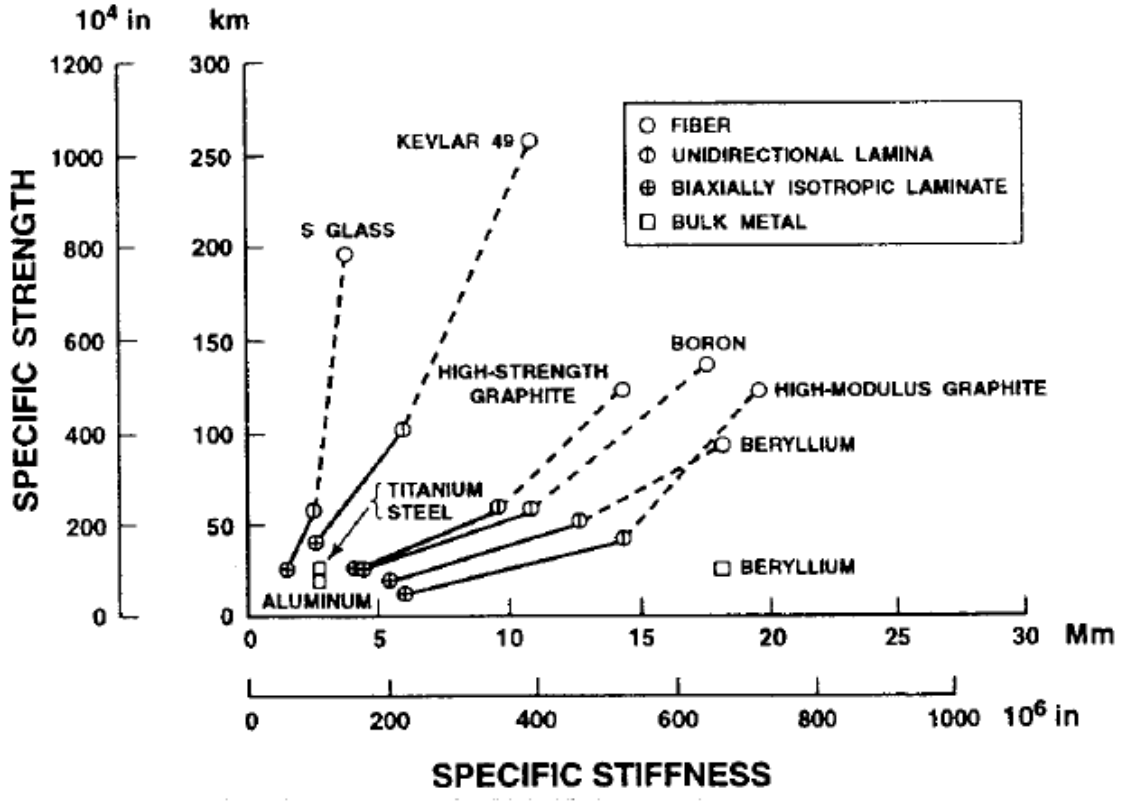

Figure 1.1 - Specific stiffness and strength comparison between the composites and metals (reproduced from Ref. 14)

Beyond a clear advantage of the high specific strength and stiffness, other benefits of using composites are their vanishing conductivity (mostly, with some exceptions e.g. carbon-fiber), improvement in fatigue resistance, corrosion prevention and others such as potential fabrication cost advantages for parts with complex shapes or performance (e.g. damage tolerance). But there are also disadvantages, as composite parts are difficult to inspect and when damaged, they are usually hard to repair, so the whole part may have to be replaced. Making the decision to repair or replace is not so straightforward.

Due to the adaptability of composites to different situations, the applications for composites are quite wide including boat decking, transport, civil engineering, general engineering, aerospace and sports. They provide ample scope and receptiveness to design changes, materials and processes.

In aviation composites have been experimented since the 1920s, but the situation was held for many years without a proper material for production. In the 1950-60s glass fiber reinforced plastics (GFRP) were introduced. These are not appropriate for structural applications with heavily loaded aircrafts, such as commercial or high performance aircrafts. Nowadays advanced composite materials such as carbon fiber reinforced plastics (CFRP) or boron reinforced plastics (BFRP) are used for these applications. For light loaded aircrafts aramid reinforced plastics are used, they possess a high tensile strength, however a low compressive strength. Also glass fiber is an option for the light loaded aircrafts.

The evolution of composite material allowed the development of complete FRP airframes. This follows with weight saving, with improvement in performance, durability, corrosion prevention and drag reduction. This naturally leads to the reduction in operating costs due to fuel saving.

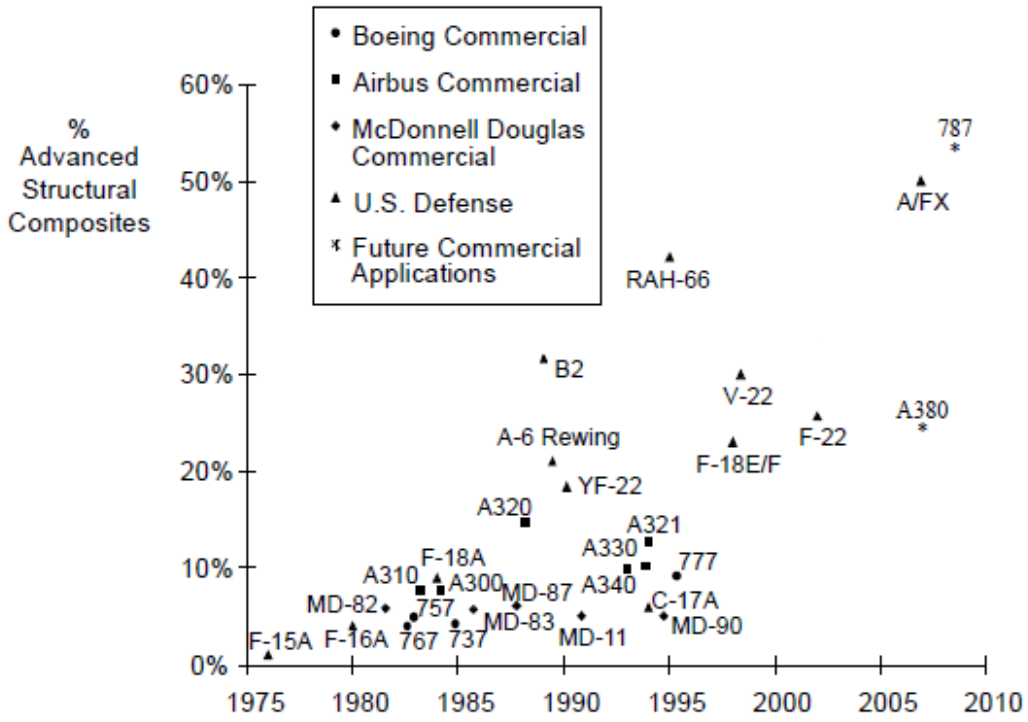

Figure 1.2 – Evolution of composite usage in structural weight in aviation (reproduced from Ref. 13)

An example of such application is Boeing 787 Dreamliner (Figure 1.2), the first full-size commercial aircraft with composite wings and fuselage. The estimated composite structural weight is 50% and a 19:1 part reduction. In contrast, Boeing 777 consists of only 12% of the composite structural weight. [10]

The development of composite materials is a time consuming process as compatible base material A and B must be developed. Therefore time to market for composite materials is also long. Unlike aluminium, composite materials require a more extensive certification process and more tests are required.

For future research and development other enabling technologies are needed for better structural performance. Enabling technologies include process molding, material property prediction, failure prediction and damage modeling. Breakthrough in manufacturing technologies is needed to reduce significantly the production cost. [27]

1.3. Failure mechanisms

The failure mechanisms in fiber-reinforced composite (FRC) materials include delamination, intralaminar matrix cracking, longitudinal matrix splitting, fiber/matrix debonding, fiber pull-out, and fiber fracture.

With unidirectional composite material, when a tensile load is applied in the direction of the fibers, these tend to rupture first, because the allowable strains for the fibers is smaller than to those of the matrix. Depending on the fiber volume fraction, the matrix might be able to support the load. Local failure modes will occur at a much lower stress level (e.g. 50% of ultimate strength), such as fiber pull-out, debonding of fibers, interface-matrix shear failure, etc. Compressive loading can cause stress concentration on the matrix around the fibers due to the Poisson effect. Then fiber matrix interface failure or transverse splitting may occur. Again, the failure mode is also dependent on the fiber volume fraction, because when fibers act independently and are further away from each other, fiber buckling may occur, otherwise fiber-kinking.

It was explained what happens with loadings in the fiber direction (longitudinal loading). As for the transverse tensile loading, the final strength is even lower than of the matrix alone as there are stress concentration due to the fibers, because they are constraining the matrix. With compressive transverse loading similar effects can be observed, the associated failure mode is usually matrix shear failure accompanied with debonding. At last, the in-plane shear loading failure mode is very much dependent on the fiber-matrix interface strength. If the interface is weak then the failure doesn't depend on the fibers or the matrix.

With laminates, which are constituted of several plies and bonding interfaces between them, it is not so straightforward to understand the failure. It can occur on both, on the ply or on the interface. Interface failure would cause delamination to occur. Ply failure can occur in different forms as referred above and is very much dependent on the stress state and load case. Therefore when dealing with a laminate, the stress concentration and stress distributions are different. The analytical solutions that have been developed for individual plies are not sufficient to describe failure in laminates. Therefore, in classical lamination

theory there are several criteria to predict first ply failure (based on intralaminar stresses) or delamination (based on interlaminar stresses).

First-ply-failure (FPF) is not always sufficient for the failure analysis, because the failure of a ply does not necessarily mean the failure of a whole structure. Often the stresses are redistributed in such a way that the structure does not fail and a new crack may or may not initiate in another position. More details on failure mechanisms can be found in Ref. 22.

1.4. Scope of the present work

As referred earlier, laminates allow interesting applications, therefore the numerical study of their properties becomes important for their development. In the study of laminates it is important to model damage to predict failure. For this purpose the finite element method is used with the general purpose FEM package ABAQUS/Standard 6.11 (*Dassault Systèmes Simulia Corp., Providence, RI, USA*).

In the preceding section, it was stated that the FPF is not always sufficient. A modeling strategy which allows to model damage further after FPF is intended, where delamination can also occur. In this thesis, damage modeling of the ply and of the interface is performed, allowing the interaction between them. The behavior of this modeling strategy is linear just until the first-ply-failure or interface failure, afterwards it is non-linear due to stiffness degradation from damage evolution.

1.4.1. Linear elastic behavior

Regarding the linear elastic behavior, modeling the interface in ABAQUS should not, in theory, affect the overall stiffness of the laminate, but this may not be the case, as results were found with similar tests where the transverse shear stiffness was overestimated when modeling with conventional shell elements with a cohesive surface for the interface [16]. For a better understanding of how the latter influences the transverse shear and bending stiffness (even though conventional shell elements are quite good in dealing with bending), a 3-point bending model is considered with a 0/90 ply lay-up on a laminate. The reason is

the relative simplicity of this model, therefore avoiding additional geometric complexity, and the availability of an analytical solution. The beam when deformed, in the 3-point bending test, has a contribution from bending and from transverse shear. The length-to-thickness ratio determines the percentage of contribution from each. By changing the boundary conditions, different characteristic lengths are used, where effects of transverse shear are higher. This is desired, to verify if the modeling strategy also works well when dealing with high transverse shear loads. Even though the transverse shear isn't considered in to the damage model, there is a linear superposition in the displacement contributions from bending and transverse shear, therefore the amount of bending will also be different. The interest in the elastic behavior is justified by the fact that accurate computation of stresses and stiffness is important for FPF, as it is the first step in damage modeling.

The stiffness of the conventional shell elements model is compared not only with the analytical solution, but also with the 2D fully integrated continuum elements and continuum shell elements. Continuum elements provide quite accurate results, but they require a more refined mesh as they do not have rotational degrees of freedom. In the end, for continuum elements the total number of degrees of freedom is higher, making the computation more expensive. Continuum shell elements are interesting, because their formulation is somewhere in between continuum elements and conventional shell elements. Visual representation of the models can be seen in Figure 1.3. More details will be given in Chapter 3.

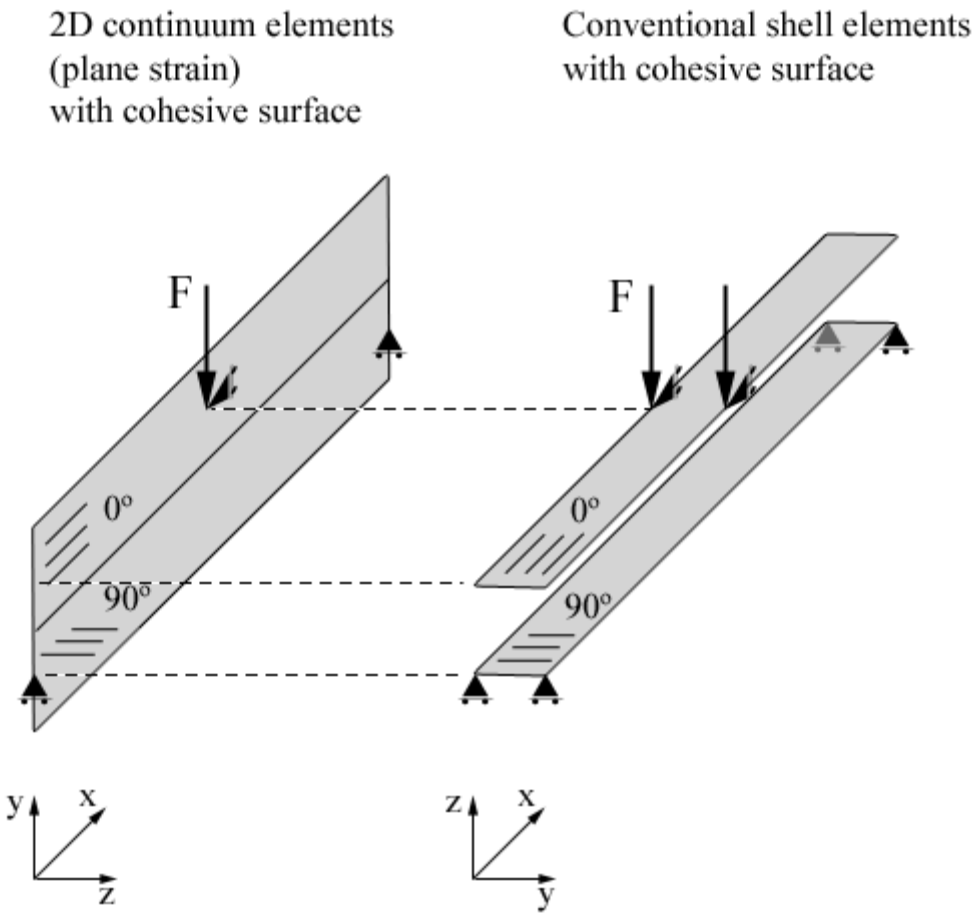

Figure 1.3 – Modeling approach for layered composite beam with 2D Continuum elements in plane strain and two layer conventional shell elements. The comparison between the models is established by applying equivalent boundary conditions.

1.4.2. Damage modeling

For this part of the thesis, the question is whether the damage is computed correctly and if ply failure interacts correctly with delamination. Again, the 3-point bending test with 0/90 orientation is adequate, because the expected behavior (with a long beam and significant contribution from bending) would be a crack growing from the bottom on the center of the beam. When the 90º layer fails through the thickness of the ply until the interface surface, then delamination should occur, see Figure 1.4. For a short thick beam the results are not so clear, because even though transverse shear is not included in the damage model, there could still be indirect influence on the damage modeling.

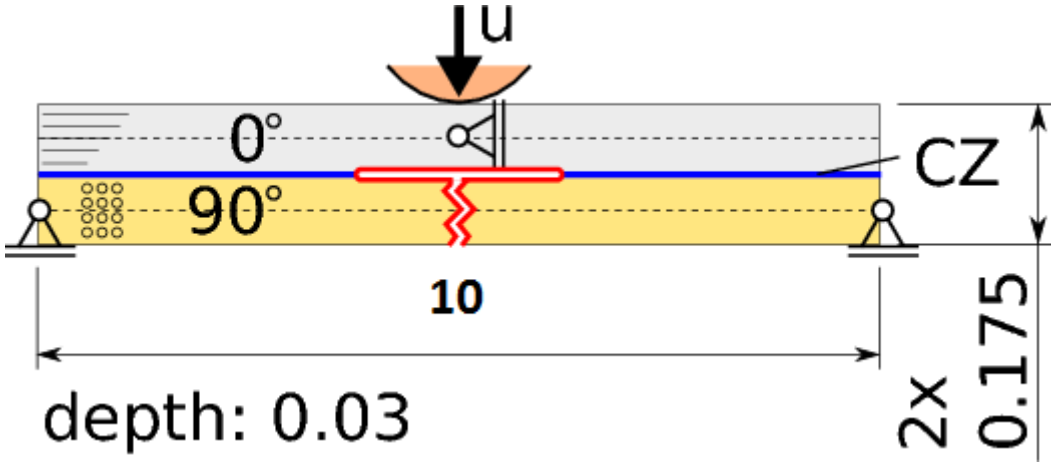

Figure 1.4 – Expected damage progression in a 3-point bending test on a cross-ply laminate (reproduced from Ref. 17)

Unfortunately, there is no experimental data to compare the results. Since modeling damage is a non linear computation, there are no analytical solutions to compare with our data. Also there is no damage model for continuum elements in plane strain. Therefore, it is of interest to find a configuration where failure occurs in a clear sequence of events, this way creating the possibility for a future experiment for the purpose of comparing experimental and modeling data. Recommendations are taken from EN ISO 14125, although not strictly followed, for the lay-up computed for the future experiment.

1.4.3. Content summary

Chapter 2 presents the theory behind the elastic behavior of the beam. The Euler beam describes how to obtain the deflection from bending by applying a vertical load at the center of a beam. The Timoshenko beam extends the solution with a larger deflection due to bending and first order transverse shear contributions. Finally, lamination theory is required to calculate the stiffness matrices of the 0/90 layer composite beam, as originally the Euler and Timoshenko beam analytical solutions are given for homogeneous beams. The analytical solutions are obtained to calculate the maximum deflection by applying a concentrated load on a 3-point bending configuration.

Chapter 3 provides the detailed description of the modeling used to build the finite element model. Specimen size, element size, loading rate, applied displacement, the punch modeling and boundary conditions are defined. In addition the boundary conditions are set

so that the shell element model can be compared with the continuum element model in plane strain. Material data is defined, including the damage model for the ply and the interface. Also a model with continuum shell elements is defined for comparison. Finite element formulation that is relevant for the modeling is explained in this chapter.

The results of the calculations are presented in Chapter 4. At first, the results concerning the initial model (the elastic behavior with different elements types) are presented, then follows the damage modeling complemented with a comparison between the continuum and conventional shells. In the second part of the Chapter are presented the computational results within the experimental model, with a realistic geometry of the specimen. The force-displacement plots are presented along with discussion and relevant figures presenting the results.

Finally, Chapter 5 contains the final conclusions and remarks of the thesis.

1.5. Literature review

The literature review presented in this work is based on a review – thesis by Lista [16], because the damage modeling strategy, ply and interface damage models and material parameters are the same ones as used in [16].

Classical lamination theory serves as a basis for the understanding of laminates. It is required to obtain effective stiffness based on their lay-up, to understand the simplifications and assumptions made. Therefore, a textbook on the topic by Jones [14] is recommended.

Regarding ply damage, the first-ply-failure prediction is required. One of the most known criteria was developed by Puck [18]. Later, it was extended by Puck and Schürmann [19] and Knops [20]. This criterion is quite accurate and is based on classical lamination theory (details are given in [22]). The distinction is made between the fiber failure and matrix dominated failure. It is based on the Mohr's fracture hypothesis. It was first used by Hashin [11] for uni-directional composites where four failure modes are considered fiber tension, fiber compression, matrix tension and matrix compression.

In the present thesis, the Hashin criterion is used for modeling the ply damage with ABAQUS and it is included in the FEM package. The damage initiation model was developed by Lapczyk [15]. The damage evolution model is a simplification of the model developed by Camanho and Davila [6] for interlaminar stresses. The latter is an energy approach which accounts for the stiffness degradation through the release of energy due to damage. There is another damage model developed in the Institute of Lightweight Design and Structural Biomechanics (ILSB) in Vienna University of Technology, which is based on the Puck criterion. The ILSB damage model was developed by Schuecker and Pettermann [24, 25] and Flatscher and Pettermann [7].

More details on the validity of current ply failure theories can also be found in [12] or in a recent review on current progressive degradation damage models [9].

Regarding delamination, several studies have been concluded on natural composites in 1980's. It was the starting point in the field of delamination. The origin and growth of delamination in stability problems was performed by Garg [8] and Bolotin [4]. In this thesis the traction-separation approach is adopted, with a quadratic strength criterion for damage initiation on the interface. Later studies have been performed by Brewer [5]. As for damage evolution, mixed energy modes are used introducing an effective displacement, see Ref. 6 for details. When the critical fracture energy is the same along the first and second shear direction during deformation, then the criterion by Benzeggagh and Kenane [3] were useful. The same criterion is used in the present thesis.

In order to avoid the introduction of a delaminated area, even though computationally more expensive, methods such as the introduction of a cohesive zone element to model the interface [2] are used.

2. Theoretical background

2.1. Euler Beam

The Euler beam allows to predict the load or the deflection under bending and the stress and strain fields as well. Therefore, it is only valid for high length-to-thickness ratios, when the contribution from transverse shear is negligible. It is valid under the assumptions of small strain and small rotations. Classical beam theory describes the elastic behavior through Hooke's law, which was originally meant for homogeneous beams, the solution can be extended for composite beams in combination with lamination theory. This section follows the content adapted from Ref. 29.

The Euler beam theory describes the elastic behavior of the beam. The deflection can be calculated, as well as the moments and forces, which in posterior allow computing the stresses. The stress distributions just with consideration of bending are normal stresses, which are maximum on the surface of the beam. Depending on the loading direction the maximum tensile stresses are on the upper or lower layer and on the opposite surface the maximum compressive stresses. Naturally, in our example, as the maximum bending moment is on the center of the beam, the stress concentration is also in the center. This is important for understanding, why would the 0/90 layer composite beam fail at first on the lower ply surface with a significant contribution from bending.

The differential equation for the static beam is

$$\frac{d^2}{dx^2}\left(EI\frac{d^2w}{dx^2}\right) = q\,, \qquad \text{(Eq. 2.1)}$$

where E is the Young modulus, I is the second moment of inercia and w is the deflection with a certain distributed load q.

The curvature is defined as

$$\theta = \frac{dw}{dx}, \qquad \text{(Eq. 2.2)}$$

and the curvature change as

$$k = \frac{d^2w}{dx^2}. \qquad \text{(Eq. 2.3)}$$

The curvature change is required to describe the bending moment:

$$M(x) = -EI\frac{d^2w}{dx^2}. \qquad \text{(Eq. 2.4)}$$

The analytical solution for a 3-point bending with a concentrated load in the middle is obtained. The analytical solution for the maximum deflection is

$$w = \frac{PL^3}{48EI}, \qquad \text{(Eq. 2.5)}$$

where P and L are defined as represented on Figure 2.1.

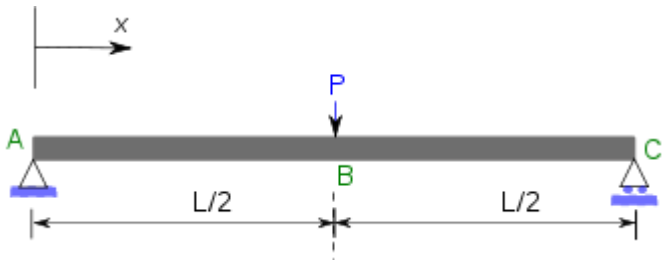

Figure 2.1 – 3-point bending beam (reproduced from Ref. 29)

2.2. Timoshenko beam

From the analytical solution of the Euler beam, it is calculated only the contribution from bending of the vertical load (with a known displacement). The deflection, without transverse shear considerations for a beam with low length-to-thickness ratio, will be under predicted. But with the Timoshenko beam theory, this contribution is calculated, making it compatible for the analysis of short thick beams [26]. The ordinary differential equations governing the behavior are,

$$\frac{d^2}{dx^2}\left(EI\frac{d\theta}{dx}\right) = q \qquad \text{(Eq. 2.6)}$$

and

$$\frac{dw}{dx} = \theta - \frac{1}{kAG}\frac{d^2q}{dx^2}. \qquad \text{(Eq. 2.7)}$$

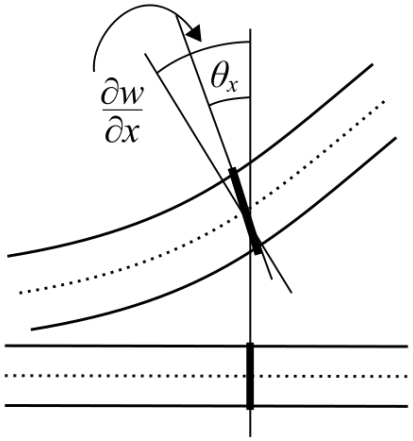

Figure 2.2 – Shear contribution on the angle in the Timoshenko beam (reproduced from Ref. 28)

Some similarities can be observed with the Euler beam, except that, $\frac{dw}{dx}$ is no longer equal to θ, because there is another contribution to the angle now from the transverse shear, as see Figure 2.2. Therefore the angle is no longer perpendicular to the deformed beam axis. In a situation where there is only shear deformation (pure shear) the angle does not change in comparison to its original configuration.

The analytical solution of the Timoshenko beam [26], for the beam shown in Figure 2.1, as described in the previous section is

$$w = P\left(\frac{L}{4kAG} + \frac{L^3}{48EI}\right) \qquad \text{(Eq. 2.8)}$$

where k is the shear correction factor, ABAQUS uses $k = 5/6$ as standard for shells (true assumption for the homogeneous beam, but for the composite beam other values have to be adopted), A is the area of the cross-section of the beam. The shear modulus G can be defined for isotropic material as

$$G = \frac{E}{2(1+v)}, \qquad \text{(Eq. 2.9)}$$

where v is the Poisson ratio.

In Equation 2.8, the first term in the brackets is due to transverse shear contribution and the second term is due to bending.

2.3. Lamination theory

As referred earlier lamination theory deals with the material parameter prediction of laminates such as stiffness, based on the ply lay-up or failure prediction with first ply failure (FPF) criteria. Interlaminar stresses are also evaluated. This section follows ideas outlined in Ref. 22.

The constitutive relations of the individual uni-directional (UD) layer are defined as

$$\sigma_L = \begin{pmatrix} \sigma_{ll} \\ \sigma_{qq} \\ \tau_{lq} \\ \tau_{lt} \\ \tau_{qt} \end{pmatrix} = \begin{pmatrix} (E_{11})_L & (E_{12})_L & 0 & 0 & 0 \\ & (E_{22})_L & 0 & 0 & 0 \\ & & (E_{44})_L & 0 & 0 \\ & & & (E_{55})_L & 0 \\ sym. & & & & (E_{66})_L \end{pmatrix} \begin{pmatrix} \varepsilon_{ll} \\ \varepsilon_{qq} \\ \gamma_{lq} \\ \gamma_{lt} \\ \gamma_{qt} \end{pmatrix}, \qquad \text{(Eq. 2.10)}$$

where the subscript L refers to the local orthotropy axes, which are l and q, referring to longitudinal (fiber direction) and transverse direction respectively. The out-of-plane direction is t. There are no normal out-of-plane components (only the first-order shear components) as plane stress state is assumed for laminas. The normal stresses are defined as σ, the shear stresses as τ, the normal strains ε and the shear angles as γ with the respective subscripts (each stress or strain component has a direction associated to it).

The individual components $(E_{11})_L$, $(E_{12})_L$ and $(E_{22})_L$ are normal in-plane parameters. $(E_{44})_L$ is the in-plane shear parameter. The other two parameters $(E_{55})_L$ and $(E_{66})_L$ are the transverse shear in the longitudinal and transverse direction. In certain cases these can be removed, as for long thin plates or shells where bending is the predominant loading. The individual components are further defined as

$$\begin{aligned}
(E_{11})_L &= \frac{E_l}{1-(v_{lq})^2\frac{E_q}{E_l}} \\
(E_{22})_L &= \frac{E_q}{1-(v_{lq})^2\frac{E_q}{E_l}} \quad , \\
(E_{12})_L &= v_{lq}(E_{22})_L \\
(E_{44})_L &= G_{lq} \\
(E_{55})_L &= G_{lt} \approx G_{lq} \\
(E_{66})_L &= G_{qt} \approx G^{Matrix}
\end{aligned} \qquad \text{(Eq. 2.11)}$$

where v_{lq} is the in-plane Poisson ratio, G_{lq} is the in-plane shear modulus, G_{lt} and G_{qt} are the out-of-plane shear modulus in the longitudinal and transverse direction respectively, E_l refers to the longitudinal Young modulus and E_q to the transverse Young modulus.

The deformation behavior of the UD-layer is described by the plate and shell theory by Reissner [23]. Shear out-of-plane deformations are considered without any normal (out of plane) deformations. These considerations are the same as in the Timoshenko beam except that it can be applied to plates. The difference is that there are two angles, because two transverse shear directions are considered. The strains for the Mindlin-Reissner kinematics are defined as:

$$\begin{aligned}\overline{\varepsilon}^T &= \left(\frac{\partial \bar{u}_1}{\partial x_1}, \frac{\partial \bar{u}_2}{\partial x_2}, \frac{\partial \bar{u}_1}{\partial x_2} + \frac{\partial \bar{u}_2}{\partial x_1}\right) \\ x^T &= \left(\frac{\partial \theta}{\partial x_1}, \frac{\partial \varphi}{\partial x_2}, \frac{\partial \theta}{\partial x_2} + \frac{\partial \varphi}{\partial x_1}\right) \\ \gamma^T &= \left(\frac{\partial \bar{u}_3}{\partial x_1} - \theta, \frac{\partial \bar{u}_3}{\partial x_1} - \varphi\right)\end{aligned} \quad , \qquad \text{(Eq. 2.16)}$$

where $\overline{\varepsilon}$ describes the strains of the mid-surface, x are the curvature changes, γ are the transverse shear angles, $\overline{u}$ are the mid-surface displacements, θ is the longitudinal angle and φ is the transverse angle.

After the behavior of individual UD layers has been defined, the elasticity matrix of each layer must be rotated relative to the global axes through the rotation matrix, following the equations

$$\boldsymbol{T}(\alpha) = \begin{pmatrix} c^2 & s^2 & 2sc & 0 & 0 \\ s^2 & c^2 & -2sc & 0 & 0 \\ -sc & sc & c^2 - s^2 & 0 & 0 \\ 0 & 0 & 0 & c & s \\ 0 & 0 & 0 & -s & c \end{pmatrix} , \qquad \text{(Eq. 2.12)}$$

and

$$E = \boldsymbol{T}^{-1}(\alpha)\, \boldsymbol{E_L}\, (\boldsymbol{T}^T(\alpha))^{-1} \ , \qquad \text{(Eq. 2.13)}$$

where α is the fiber orientation angle, c is $\cos(\alpha)$ and s is $\sin(\alpha)$

The stiffness matrices are defined as

$$\begin{aligned}
\boldsymbol{A} &= \sum_{n=1}^{N} {}^{n}\boldsymbol{E}\left({}^{n}x_3 - {}^{n-1}x_3\right) = {}^{n}E\,{}^{n}h \\
\boldsymbol{B} &= \sum_{n=1}^{N} {}^{n}\boldsymbol{E}\left(\frac{{}^{n}x_3^2 - {}^{n-1}x_3^2}{2}\right) \\
\boldsymbol{D} &= \sum_{n=1}^{N} {}^{n}\boldsymbol{E}\left(\frac{{}^{n}x_3^3 - {}^{n-1}x_3^3}{3}\right) \\
\boldsymbol{A^t} &= \sum_{n=1}^{N} k\,{}^{n}\boldsymbol{E}^{t}\left({}^{n}x_3 - {}^{n-1}x_3\right) = k\,{}^{n}E\,{}^{n}h
\end{aligned} \quad , \qquad \text{(Eq. 2.14)}$$

where *n* refers to the ply number, *N* is the total number of plies, *h* is the ply thickness, x_3 is the out-of-plane coordinate from the mid-surface, $\boldsymbol{E}$ is the elasticity matrix without out-of-plane consideration, and $\boldsymbol{E^t}$ are the last two terms of the elasticity matrix for the transverse shear directions. In the matrix $\boldsymbol{A^t}$ the shear correction k must be specified for both the first and second directions. For more details on shear corrections factors for laminates see Ref. 21.

The constitutive behavior of laminates can be defined as

$$\begin{aligned}
\begin{pmatrix} N \\ M \end{pmatrix} &= \begin{pmatrix} \boldsymbol{A} & \boldsymbol{B} \\ \boldsymbol{B} & \boldsymbol{D} \end{pmatrix} \begin{pmatrix} \bar{\varepsilon} \\ \chi \end{pmatrix} \\
Q &= \boldsymbol{A^t}\gamma
\end{aligned} \quad , \qquad \text{(Eq. 2.15)}$$

where *N*, *M* and *Q* are the normal stress resultants, bending moment stress resultants and transverse shear stress resultants vectors, respectively, for the directions defined in the Equation 2.10.

With all UD-layers defined in the global axes, the stresses can be integrated over the thickness to obtain the stress resultants for the laminate. The terms are then reorganized to form the stiffness matrices $\boldsymbol{A}$, $\boldsymbol{B}$ and $\boldsymbol{D}$. These matrices are called extensional, coupling and bending stiffness matrices, respectively. This way of solving laminates is more interesting, because if the coupling matrix $\boldsymbol{B}$ is not zero, then coupling between extension and bending

can be observed, such as bending in a cross-ply or warping in a ply-angle laminate. To avoid this effect, symmetric laminates can be made by creating the same plies from the mid-surface, this means same $\boldsymbol{E_L}$, same thickness and same orientation α. Quasi-orthotropic laminates for pure in-plane loading can be defined if the terms A_{14} and A_{24} are zero. For 0º and 90º orientations they are indeed zero. For other angles, for each lamina with $+\alpha$ must exist a $-\alpha$ angle. By using 0º or 90º plies or by using alternate angle-plies, it is possible to achieve a structure where there is no coupling between normal stresses and shear strains. The same effect is observed in the bending stiffness matrix $\boldsymbol{D}$ for the terms D_{14} and D_{24}, except here the angles must be alternating in respect to the mid-surface, making it hard to achieve symmetric laminates, except for cross-ply laminates. The solution is the usage of many thin plies in an angle-ply, which would make the terms nearly zero, achieving homogeneous orthotropic behavior.

In a short note, lamination theory does not provide a good prediction for the stresses near the free edges, where they are supposed to be zero (not all the components). The farther away from the edges, the less pronounced this effect is.

3. Modeling

3.1. Overview

The damage model, contact model and geometric discretization model used in this thesis are integrated in the ABAQUS FEM package.

With traditional modeling strategies, where only FPF is intended, composite sections are applied to shell elements. With composite sections the assumption is the same as with classical lamination theory – the interface is perfect. In the context of this work, in order to model delamination, the interface is damageable. So each ply is modeled as an individual shell layer. By assigning a surface (or two surfaces, depending on the amount of layers) to each shell layer, it is possible to couple them together through a cohesive surface. The latter is modeled with a traction-separation approach, so the thickness of the interface is assumed to be zero. Then, a damage model can be defined, creating a damageable interface as required. Additionally, contact formulation must be assigned with a master and a slave surface, for this a small sliding approach is chosen, meaning that the nodes from the slave should not slide further away than the corresponding element from the master surface. Choosing which surface in the laminate is master and slave has a significant influence over damage modeling, which is some sort of defect in ABAQUS. Also the damage model is defined for the ply material, which would also be the same as for composite sections.

3.2. Element type

The three element types used in the present thesis are conventional shell elements (S4), continuum shell elements (SC8R), and 2D continuum elements (CPE8R). The theory presented in this section follows the ABAQUS Manual [1].

3.1.1. General purpose shell elements

General purpose shell elements (S4) are appropriate for structural applications as one direction is considered to be smaller than the other. Therefore, plane stress is imposed, allowing reduced number of degrees of freedom and computation time. Since conventional shell elements possess rotational degrees of freedom, they can reproduce bending quite accurately, because of this, they do not require such a refined mesh as continuum elements. Composites also have the thickness direction (the ply thickness) smaller than the other directions, making conventional shell elements suitable for this application. Even though plane stress assumption is made, there is still variation of thickness due to the Poisson effect, but only when finite strain formulation is adopted. In ABAQUS this is achieved by using non-linear geometry.

S4 elements are valid for thin and thick shells, which allow for the first-order shear deformation. The rotational degree of freedom is computed normal to the surface reference and then deformed depending on the amount of transverse shear. But, when Kirchhoff theory isn't applied as in thin shell theory, then shear locking may occur in the transverse direction. For this, ABAQUS uses a dimensionless factor to prevent the transverse shear stiffness becoming too large in thin shells, which depends on the element area and shell thickness. The effective transverse shear is defined as,

$$\overline{K}_{\alpha\beta}^{ts} = f_p K_{\alpha\beta}^{ts} \,, \qquad \text{(Eq. 3.1)}$$

where $K_{\alpha\beta}^{ts}$ is the actual transverse shear stiffness calculated by Abaqus. α and β refer to the surface directions on the shell. The dimensionless factor is defined as,

$$f_p = 1/(1 + 0.25 * 10^{-4} \frac{A}{t^2}) \,, \qquad \text{(Eq. 3.2)}$$

which is dependent on the element size *A* and the shell thickness *t.*

Also an assumed strain method based on the Hu-Washizu principle is used for the treatment of transverse shear. In the mid-surface of S4 elements there are 4 integration

points inside the element and linear interpolation is used. By combining the original integration points (Figure 3.1) with the new points (Figure 3.2) a new strain field can be obtained, which is much more immune to overestimated values of transverse shear.

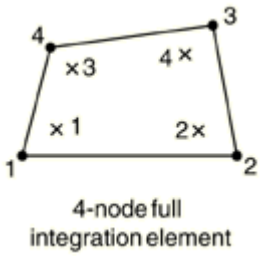

Figure 3.1 – Conventional shell elements S4 (reproduced from Ref. 1)

For this, the transverse shear strains are obtained from the original and deformed shell normals for the points A, B, C and D as represented on Figure 3.2. Then they are averaged into to strain fields for the first and second shear directions.

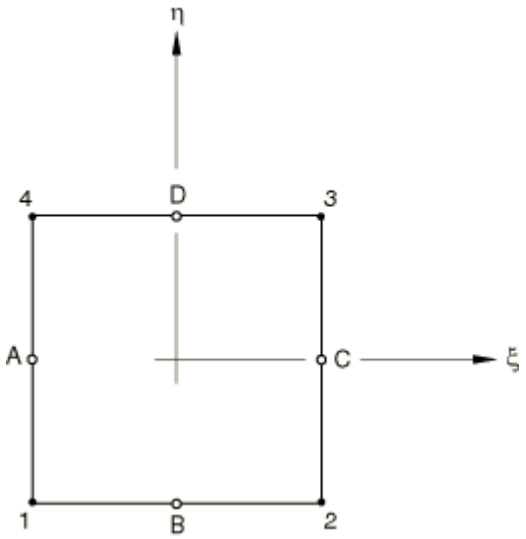

Figure 3.2 – Shell midsurface (reproduced from Ref. 1)

Now, the transverse shear forces are obtained from the St. Venant-Kirchhoff constitutive model for the Kirchhoff curvilinear components,

$$\begin{Bmatrix} Q_1 \\ Q_2 \end{Bmatrix} = \boldsymbol{C_s} \begin{Bmatrix} \overline{\gamma}_1 \\ \overline{\gamma}_2 \end{Bmatrix} \qquad \text{(Eq. 3.3)}$$

where the strain fields $\overline{\gamma}_1$ and $\overline{\gamma}_2$ for both transverse shear directions, Q_1 and Q_2 the respective shear forces. The transverse shear stiffness $\boldsymbol{C_s}$ for an isotropic plate is defined as,

$$\boldsymbol{C_s} = \frac{5}{6} G_s h \begin{bmatrix} A^{11} & A^{12} \\ A^{21} & A^{22} \end{bmatrix}. \qquad \text{(Eq. 3.4)}$$

When specified, the section properties are integrated throughout the analysis. Then the properties throughout the thickness, such as the stiffness for in-plane bending and out-of-plane shear response are computed, because output data is required not only on the mid-surface of the shell element. For that integration points are specified, the amount depends on the accuracy required. Naturally, more integration points will lead to a longer computation time. As for the integration, there are two schemes available in ABAQUS - the Gauss quadrature and Simpson's rule. The Gauss quadrature has no integration point on the shell surfaces, but has a higher accuracy with the same number of integration points than the Simpson's rule. In this thesis the Simpson's rule is used as output is required for the shell surfaces.

As for stress output, the conventional shell elements are quite accurate for the in plane components as these are obtained from the constituent parameters of the material. Which is no longer the case for transverse shear stresses – the strain energy from the transverse shear deformation is equated to the transverse shear stress distribution energy of a unidirectional beam bending (parabolic distribution, with maximum value on shell mid-surface and zero on outer surfaces of the shell). The transverse shear stiffness for composite sections is also calculated by these means. In the shell formulation only first-order shear strains are considered within the rotational degree of freedom, just as in the Timoshenko beam or Mindlin plate theory. Therefore they require a shear correction factor, which for homogeneous plates is well known to be 5/6, providing quite accurate results. But for the composite sections Abaqus has to recalculate this value to provide a more correct estimate, when using non-symmetric laminates, the transverse stiffness and stresses can be less accurate as the shell section directions are considered to be the principal bending directions. Abaqus computes the transverse shear stiffness only once at the beginning of the analysis based on the elastic properties. Any changes that occur in the

transverse shear stiffness due to changes in the material stiffness during the analysis are ignored.

3.1.2. Continuum shell elements

The continuum shell elements do not have rotational degrees of freedom as the conventional shells and are only available with reduced integration, making them susceptible to “hourglassing”, for this purpose ABAQUS uses hourglass control for such elements. Each element is defined by 8 nodes, in contrast to conventional shells where only the mid-plane surface is defined. The integration point is in the middle of the element, as shown in Figure 3.3. Continuum shell elements use finite strain formulation.

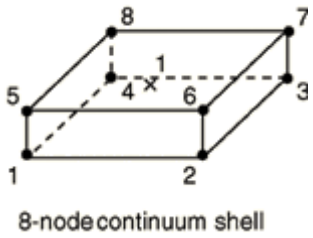

Figure 3.3 – Continuum shell elements SC8R (reproduced from Ref. 1)

The section for continuum shell elements is specified in the same way as for conventional shell elements (Gauss quadrature or Simpson’s rule as integration schemes), with integration points over the thickness and the calculation of transverse shear stresses and the shear correction factor is the same as for conventional shells, with unidirectional bending over one axis to equate the strain energy. The exception is for specifying the thickness, which is done with nodal coordinates, instead of in the shell section. The ply thickness specified in the section will be used for other section properties, such as hourglass control.

3.1.2. 2D plane strain continuum elements

CPE8R are 8-noded bi-quadratic elements in plane strain with reduced integration. The high amount of bending in the elements was the reason for using bi-quadratic elements, therefore allowing them to assume a curvilinear shape. As referred earlier, the continuum elements can compute accurately the stresses and forces for bending and transverse shear

load cases, but their use does not go that far, because there is no damage model for continuum element in plane strain and 3D continuum elements are too expensive.

The nodes in these elements have 2 degrees of freedom and must be defined in the x-y directions (one and two). The node and integration point locations on the element can be seen in Figure 3.4.

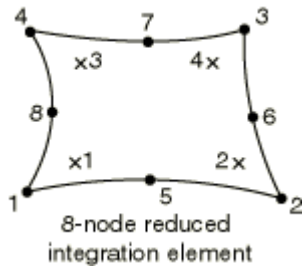

Figure 3.4 – 2D continuum elements in plane strain CPE8R (reproduced from Ref. 1)

3.2. Bonding interface

To model the bonding interface a cohesive surface behavior is used. The other option would be to use cohesive zone elements (CZE), but since conventional shell elements for ply modeling use no offset, there would be an additional complexity as constrains would have to be defined.

When modeling the cohesive surface behavior, the surface properties must be chosen for the two surfaces defined by the upper ply and lower ply. This is done by specifying the corresponding element set and normal direction of the surface. For conventional shells SPOS (it is the direction used with the right hand rule) or SNEG. For continuum shells the correspondent normals are S2 and S1 respectively. For 2D continuum elements it is enough to specify the element set and the faces that are in contact are used.

Then the contact formulation must be chosen for the surfaces defined earlier, such as an appropriate discretization. In ABAQUS two approaches are available, the surface-to-surface and the node-to-surface discretization. The tracking approach must be chosen as well, these include a finite-sliding approach and a small-sliding approach. A contact

property model is specified. Additionally, the initial conditions are specified as well, in order to guarantee that both surfaces are in contact in the beginning of the simulation.

The theory presented in this section follows the ABAQUS Manual [1].

3.2.1. Contact property model

For the contact property model, a "hard" pressure-overclosure relationship is chosen to minimize the penetration of the slave surface in the master surface at the constrain location, without transfer of tensile stress across the interface. With this relationship, when there is contact, then any pressure is possible on the surface, when there isn't then there is no contact pressure, as shown in Figure 3.5.

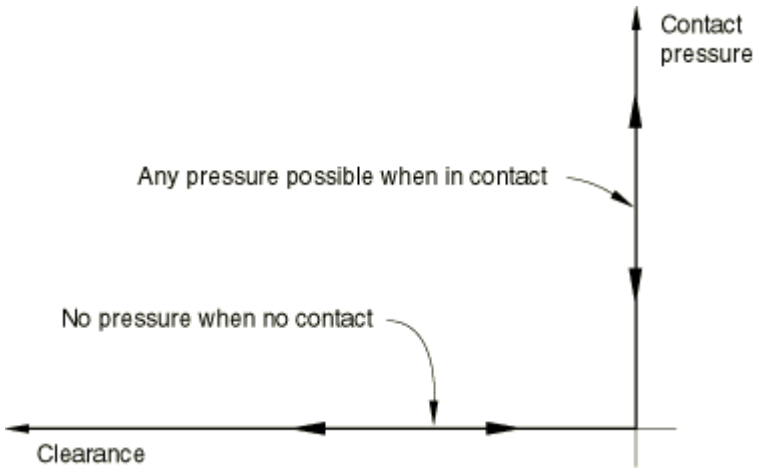

Figure 3.5 – "hard" contact pressure-overclosure relationship (reproduced from Ref. 1)

3.2.2. Contact Formulation

The node-to-surface discretization allows each node from the slave surface to interact with a group of nodes from the master surface. The slave node does not penetrate the master surface, but the master nodes can penetrate the slave surface. Within this discretization the contact direction is normal of the master surface and the geometry (normal surface direction and curvature) of the slave surface is not relevant.

With the surface-to-surface discretization there is a higher accuracy regarding the contact pressure, as it considers the geometry of both master and slave surfaces. Contact conditions are enforced in an average sense nearby an approximate slave node region. Within this formulation there is some penetration, but not large or undetected. In contrast to node-to-surface formulation, the contact direction is an average normal determined by the slave surface nearby a slave node. This formulation provides more accurate stress and pressure results, because of smoothing effects which averages over a surface instead of individual node and is less sensitive to master and slave definition than the node-to-surface formulation. Never the less, it can also be more expensive when a large fraction of model is in contact, the master surface is more refined than the slave surface or when there are multiple shell layers in contact, where one shell is master of one surface and slave of the other. In general, the surface-to-surface formulation is used in situations where normal directions of both surfaces are opposite and node-to-surface for edges or corners. For ply modeling the two surfaces have the normal direction opposite, making the choice for surface-to-surface formulation a clear option, as it provides more accurate results.

As for the tracking approach, the finite-sliding approach is the most general one and allows for arbitrary relative separation, sliding and rotation. But the small-sliding approach can be used when approximations are reasonable, providing computational savings and an added robustness. This formulation accounts for relatively little sliding, but for non--linear geometry large rotations are considered. It is based on a linearized approximation of a master surface per constrain. The group of nodes involved with the individual contact constrains are fixed throughout the analysis, but the status of the constrains can change to active or inactive. Therefore a slave node will always interact with the same area of the master surface, transferring the loads always to the same master nodes, these nodes are chosen based on their proximity from the initial configuration. Therefore, when the sliding is not “small”, naturally there will be errors in the calculation. There are pre-requisites for defining a sliding as “small”, such as that slave nodes should slide less than an element length and still be contacting their tangent plane (with a curved master surface just a fraction of an element length). Also the local tangent planes formed by ABAQUS should be a good approximation of the mesh geometry. At last, the rotations and deformation of the master surface should not cause a bad representation of the local tangent planes. Please, see Figure 3.6 for a visual representation of the local tangent plane defined on the master

surface and how deformation of the master surface can lead to inaccurate results. For the present thesis the small-sliding approach is chosen as the pre-requisites are fulfilled.

As for the master and slave surface definition, according to the ABAQUS manual, it is always better to choose the smaller surface as slave. If both surfaces have same size, then the master surface should be the stiffer (not alone in material properties, but structurally). If still no distinction between size and stiffness, then the surface with the coarser mesh should be the master surface. For this thesis, 0º and 90º layer plies are modeled. The 0º layers have a higher stiffness and should be specified as the master surface according to these rules, but the choice is not so straightforward for modeling damage as they provide a completely different response (apparently due to a flaw in ABAQUS), depending on which surface is defined as master. Further discussion on this topic will be made in Chapter 4.

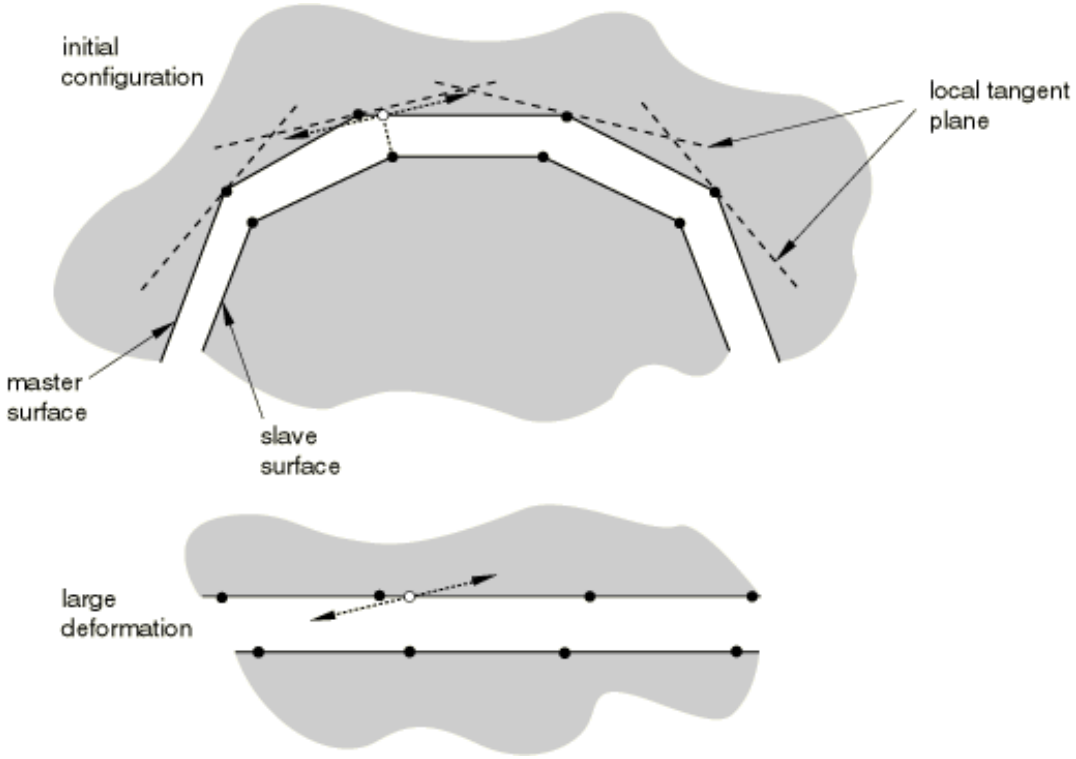

Figure 3.6 – Master surface deformation vs. local tangent plane (reproduced from Ref. 1)

3.2.3. Cohesive behavior based on a traction-separation law

The traction-separation law is intended for bonded interfaces, it is used with a cohesive surface and it is appropriate for modeling delamination. For this purpose, first the linear elastic behavior which occurs before damage is explained, then how fracture energy can be specified, in order to determine the failure of the interface characterized by progressive degradation of material stiffness.

The forces are divided by the original area at each integration point obtaining the nominal tractions. Through a constitutive elasticity matrix, defined as,

$$t = \begin{Bmatrix} t_n \\ t_s \\ t_t \end{Bmatrix} = \begin{bmatrix} K_{nn} & K_{ns} & K_{nt} \\ K_{ns} & K_{ss} & K_{st} \\ K_{nt} & K_{st} & K_{tt} \end{bmatrix} \begin{Bmatrix} \varepsilon_n \\ \varepsilon_s \\ \varepsilon_t \end{Bmatrix} = \boldsymbol{K}\varepsilon \qquad \text{(Eq. 3.5)}$$

which is a linear elastic law that relates the nominal tractions to the nominal strains, the nominal strains are then obtained. t is the traction, $\boldsymbol{K}$ the stiffness, ε the strain and the subscripts n, s and t, refer to normal, first and second shear direction respectively. The stiffness used throughout the simulations is defined as $K_{nn} = K_{ss} = K_{tt} = 10^6$ MPa.

Since the constitutive thickness defined in ABAQUS as default is 1.0, the strains correspond to the separation,

$$\varepsilon_n = \frac{\delta_n}{T_0};\ \varepsilon_s = \frac{\delta_s}{T_0};\ \varepsilon_t = \frac{\delta_t}{T_0} \qquad \text{(Eq. 3.6)}$$

where T_0 is the constitutive thickness. This thickness does not correspond to the geometrical thickness which is close to zero.

For this Master thesis an uncoupled constitutive elasticity matrix is used. Only the values for K_{nn}, K_{ss} and K_{tt} are defined, meaning that normal and shear strain will not induce traction forces in other directions than their own.

There are two parameters that must be set, damage initiation and damage evolution. For damage initiation a quadratic stress criterion is used [5], for that the tensile strength must be specified for the normal direction and the strength for the shear directions

$$\left(\frac{t_n}{t_n^0}\right)^2 + \left(\frac{t_s}{t_s^0}\right)^2 + \left(\frac{t_t}{t_t^0}\right)^2 = 1 \ , \qquad \text{(Eq. 3.7)}$$

where t^0 is the tensile strength for the different directions. When the equation is satisfied at a point in the interface, there is damage initiation that will lead to damage evolution. Notice that pure compression will not lead to damage initiation.

A linear damage evolution model is used, the mixed-mode based on an energy approach,

$$\begin{aligned} m_1 &= \frac{\mathcal{G}_n}{\mathcal{G}_T} \\ m_2 &= \frac{\mathcal{G}_s}{\mathcal{G}_T} \\ m_3 &= \frac{\mathcal{G}_t}{\mathcal{G}_T} \end{aligned} \ , \qquad \text{(Eq. 3.8)}$$

and

$$\mathcal{G}_T = \mathcal{G}_n + \mathcal{G}_s + \mathcal{G}_t \ . \qquad \text{(Eq. 3.9)}$$

There are three energy measures for the work done by traction, each measure for each direction (normal and two shear directions), $\mathcal{G}_n$, $\mathcal{G}_s$ and $\mathcal{G}_t$. Figure 3.7 illustrates how such a work measure relates to stiffness degradation.

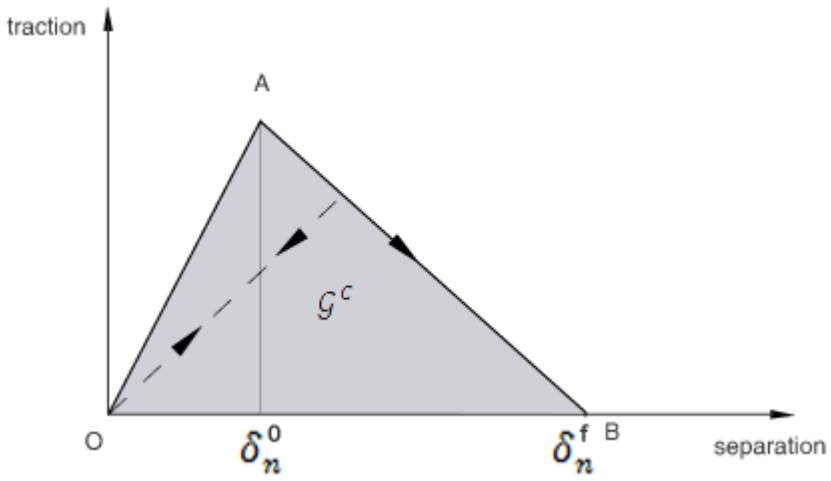

Figure 3.7 – Traction-separation law for cohesive surfaces. (reproduced from Ref. 1)

The portion of energy related shear work per area is defined as $\mathcal{G}_S = \mathcal{G}_s + \mathcal{G}_t$. When the critical energy from both directions is the same ($\mathcal{G}_s^C = \mathcal{G}_t^C$) it is particularly useful to use the Benzeggagh-Kenane approach [3]. Then the evolution law is as specified as

$$\mathcal{G}^C = \mathcal{G}_n^C + (\mathcal{G}_s^C + \mathcal{G}_n^C)\left\{\frac{\mathcal{G}_S}{\mathcal{G}_T}\right\}^\eta, \qquad \text{(Eq. 3.10)}$$

where $\mathcal{G}^C$ is the total fracture energy rate dissipated during the damage process and η is a material parameter. The value for η used in this thesis is two.

Table 3.1 lists the fracture energy rates used throughout this thesis, unless specified later otherwise and in Table 3.2 the strengths for the normal, first shear and second shear directions are presented, respectively.

$\mathcal{G}_n^C$	$\mathcal{G}_s^C$	$\mathcal{G}_t^C$
0.133	0.459	0.459

Table 3.1 – Interface fracture energy rates in J/m^2

t_n^0	t_s^0	t_t^0
60	110	110

Table 3.2 – Interface strengths in MPa

3.3. Ply material

In this section the material data, damage initiation and damage evolution for the ply material are specified and explained.

3.3.1. Elastic properties

The elastic properties of the lamina are defined in Table 3.3, with plane stress, as in Chapter 2, regarding lamination theory (Equations 2.10 and 2.11).

E_l	E_q	v_{lq}	G_{lq}	G_{qt}
146000	9000	0.34	4270	2800

Table 3.3 – Material properties of lamina in MPa

3.3.2. Damage model for ply

For fiber-reinforced composites the damage initiation criterion is given by Hashin's theory [11], it requires that the behavior of the undamaged material is linear elastic. Within this theory there are four criteria to consider four damage modes. The following are matrix tensile, matrix compressive, fiber tensile and fiber compressive damage initiation criteria respectively.

For fiber tension ($\sigma_{ll}^{eff} > 0$):

$$F_f^t = \left(\frac{\sigma_{ll}^{eff}}{X^t}\right)^2 + \alpha\left(\frac{\tau_{lq}^{eff}}{S^l}\right)^2 . \qquad \text{(Eq. 3.11)}$$

For fiber compression ($\sigma_{ll}^{eff} < 0$):

$$F_f^c = \left(\frac{\sigma_{ll}^{eff}}{X^c}\right)^2 . \qquad \text{(Eq. 3.12)}$$

For matrix tension ($\sigma_{qq}^{eff} > 0$):

$$F_m^t = \left(\frac{\sigma_{qq}^{eff}}{Y^t}\right)^2 + \left(\frac{\tau_{lq}^{eff}}{S^l}\right)^2 \quad . \qquad \text{(Eq. 3.13)}$$

For matrix compression ($\sigma_{22}^{eff} < 0$):

$$F_m^c = \left(\frac{\sigma_{qq}^{eff}}{2S^{tr}}\right)^2 + \left[\left(\frac{Y^c}{2S^{tr}}\right)^2 - 1\right]\frac{\sigma_{qq}^{eff}}{Y^c} + \left(\frac{\tau_{lq}^{eff}}{S^l}\right)^2 \quad . \qquad \text{(Eq. 3.14)}$$

Where X^t, X^c, Y^t, Y^c, S^l and S^{tr} refer to the longitudinal tensile, longitudinal compressive, transverse tensile, transverse compressive, shear longitudinal and transverse shear strength, respectively. The directions one and two from the stress components refer as well to the longitudinal and transverse directions, respectively. The coefficient α determines the contribution of shear stresses for the fiber tensile initiation criterion and the value used throughout the computations in the thesis is zero. Notice that the effective stress components are used for the criterion, which are obtained from

$$\sigma^{eff} = \boldsymbol{M}\sigma \ , \qquad \text{(Eq. 3.15)}$$

in vectorial notation, without any damage they correspond to the true stresses. The matrix $\boldsymbol{M}$ is defined as:

$$\boldsymbol{M} = \begin{bmatrix} \frac{1}{(1-d_f)} & 0 & 0 \\ 0 & \frac{1}{(1-d_m)} & 0 \\ 0 & 0 & \frac{1}{(1-d_s)} \end{bmatrix} . \qquad \text{(Eq. 3.16)}$$

The three terms d_f, d_m and d_s are damage variables. The term d_s specifies shear damage and it is dependent on other damage modes. Since there are four damage modes depending whether we have compressive or tensile stresses, they can be defined as:

$$d_f = \begin{cases} d_f^t & if\ \sigma_{ll}^{eff} > 0 \\ d_f^c & if\ \sigma_{ll}^{eff} < 0 \end{cases}$$
$$d_m = \begin{cases} d_m^t & if\ \sigma_{qq}^{eff} > 0 \\ d_m^c & if\ \sigma_{qq}^{eff} < 0 \end{cases} \qquad \text{(Eq. 3.17)}$$
$$d_s = 1 - \left(1 - d_f^t\right)\left(1 - d_f^c\right)(1 - d_m^t)(1 - d_m^c)$$

The damage variables are activated when Hashin's criterion is fulfilled. These variables grow with progressive damage evolution and stiffness degradation is achieved by equating the matrix $\boldsymbol{M}$ to the elasticity matrix $\boldsymbol{E}$, in order to obtain material parameters of the damaged material,

$$\boldsymbol{E^d} = \frac{1}{D}\begin{bmatrix} (1-d_f)E_1 & (1-d_f)(1-d_m)v_{21}E_1 & 0 \\ (1-d_f)(1-d_m)v_{12}E_2 & (1-d_m)E_2 & 0 \\ 0 & 0 & (1-d_s)G_{12}D \end{bmatrix}, \qquad \text{(Eq. 3.18)}$$

where E_1 and E_2 are the Young modulus in the fiber and matrix direction respectively and D is defined as:

$$D = 1 - (1-d_f)(1-d_m)v_{21}v_{12}\,. \qquad \text{(Eq. 3.19)}$$

In order to alleviate mesh dependency during softening, a stress-displacement constitutive model is used. The approach is based on [6], which originally was intended for modeling delamination with linear damage evolution and fracture energy dissipation. For this, the equivalent stresses and displacements are defined in the equations below.

For fiber tension ($\sigma_{ll}^{eff} > 0$):

$$\delta_{eq}^{ft} = L^c\sqrt{\langle\varepsilon_{ll}\rangle^2 + \alpha{\varepsilon_{lq}}^2}$$
$$\sigma_{eq}^{ft} = \frac{\langle\sigma_{ll}\rangle\langle\varepsilon_{ll}\rangle + \alpha\tau_{12}\varepsilon_{12}}{\delta_{eq}^{ft}/L^c}\,. \qquad \text{(Eq. 3.20)}$$

For fiber compression ($\sigma_{ll}^{eff} < 0$):

$$\begin{aligned} \delta_{eq}^{fc} &= L^c \langle -\varepsilon_{ll} \rangle \\ \sigma_{eq}^{fc} &= \frac{\langle -\sigma_{ll} \rangle \langle -\varepsilon_{ll} \rangle}{\delta_{eq}^{fc} / L^c} \end{aligned} . \qquad \text{(Eq. 3.21)}$$

For matrix tension ($\sigma_{qq}^{eff} > 0$):

$$\begin{aligned} \delta_{eq}^{mt} &= L^c \sqrt{\langle \varepsilon_{qq} \rangle^2 + {\varepsilon_{lq}}^2} \\ \sigma_{eq}^{mt} &= \frac{\langle \sigma_{qq} \rangle \langle \varepsilon_{qq} \rangle + \tau_{lq} \varepsilon_{lq}}{\delta_{eq}^{mt} / L^c} \end{aligned} . \qquad \text{(Eq. 3.22)}$$

For matrix compression ($\sigma_{22}^{eff} < 0$):

$$\begin{aligned} \delta_{eq}^{mc} &= L^c \sqrt{\langle -\varepsilon_{qq} \rangle^2 + {\varepsilon_{lq}}^2} \\ \sigma_{eq}^{mc} &= \frac{\langle -\sigma_{qq} \rangle \langle -\varepsilon_{qq} \rangle + \tau_{lq} \varepsilon_{lq}}{\delta_{eq}^{mc} / L^c} \end{aligned} . \qquad \text{(Eq. 3.23)}$$

In the equations above the $\langle \quad \rangle$ refer to the Macaulay bracket operator, which is defined for every $\langle \alpha \rangle = (\alpha + |\alpha|)/2$. Also, a characteristic length (L^c) is introduced, which is dependent on element geometry and formulation. For shell elements the characteristic length is calculated from the square root of the element area.

Now the damage factor must be obtained for each of the failure mode from the equivalent displacements,

$$d = \frac{\delta_{eq}^{f} (\delta_{eq} - \delta_{eq}^{0})}{\delta_{eq} (\delta_{eq}^{f} - \delta_{eq}^{0})} , \qquad \text{(Eq. 3.24)}$$

where δ_{eq}^{0} is the initial equivalent displacement at which damage initiates and δ_{eq}^{f} the displacement at which damage evolution is maximum. At last by defining the dissipated energy associated with each failure mode the value for δ_{eq}^{f} can be calculated:

$$\delta_{eq}^{f} = \frac{2\mathcal{G}^{C}}{\delta_{eq}^{0}} \,, \qquad \text{(Eq. 3.25)}$$

where $\mathcal{G}^{C}$ is the total fracture energy rate dissipated.

In the present thesis, for all computations, unless referred otherwise, the fracture energy rates for the failure modes fiber tensile (ft), fiber compressive (fc), matrix tensile (mt) and matrix compressive (mc) are specified in Table 3.4 and the strengths for damage initiation in Table 3.5.

$\mathcal{G}_{ft}^{C}$	$\mathcal{G}_{fc}^{C}$	$\mathcal{G}_{mt}^{C}$	$\mathcal{G}_{mc}^{C}$
89.8	78.3	0.2	0.76

Table 3.4 – Ply fracture energy rates in J/m^2

X^t	X^c	Y^t	Y^c	S^l	S^{tr}
2100	1407	82	249	110	110

Table 3.5 – Ply strengths in MPa

3.4. Local softening and damping

In unstable problems, such as softening, a negative stiffness maybe observed on the force displacement graph, this leads to convergence problems. Therefore, usually an artificial damping is required. For this, viscous regularization of the constitutive equations is used both for the interface and ply material data.

For the traction-separation law the evolution equation for the regularization process is defined as

$$\dot{D}_v = \frac{1}{\mu}(D - D_v) \,, \qquad \text{(Eq. 3.26)}$$

where μ is the viscous parameter representing the time relaxation, D is the degradation variable evaluated in the inviscid backbone model, D_v is the viscous stiffness degradation. Small value for the viscous parameter (small compared to time increment) should improve convergence rate without compromising the results. When the value is specified as zero, no viscous regularization will occur. The viscous parameter used for the interface throughout the simulations in this thesis is 0.001.

Viscous-regularization may also be applied to the damage response of elements with plane-stress formulation for fiber-reinforced materials. Except of this situation, in order to compute the damaged elasticity matrix, four stabilization parameters must be defined for each failure mode. For the present thesis the values used are defined in Table 3.6, where η is the stabilization parameter and the subscripts refer to the same failure modes already specified in the section above.

η_{ft}	η_{fc}	η_{mt}	η_{mc}
0.002	0.002	0.004	0.004

Table 3.6 – Stabilization parameters for the ply damage

It is important to refer that the viscous parameter is dependent on the loading rate. In order to keep the viscous parameter unaltered throughout the simulations, the loading rate is also maintained constant at a value of 0.5 mm/s, as this value will give the best convergence and accuracy.

3.6. Geometrical model

3.6.1. Initial model

The specimen size of the initial model had already been shown in Chapter 1 in Figure 1.4. The beam lengths used are 1 mm, 4 mm and 10 mm, as referred earlier, for this load case the beam length determines the amount of contribution from transverse shear and bending. The width used is 0.03 mm and the ply thickness is defined as 0.175 mm for a cross-ply lay-up. The units used throughout the simulations are mm, N and MPa.

The discretization is made with three element types: conventional shell elements (S4); continuum shell elements (SC8R); 2D plane strain continuum elements (CPE8R). The element size for all element types is 0.025. The out-of-plane direction of the 2D continuum elements corresponds to the plate width, which here is specified as 0.03 mm, meaning that the resulting force must consider the true thickness of the plate.

The 2D continuum model is defined in the X-Y plane, which for the shell elements corresponds to the X-Z plane. The position of the mid-surface of the conventional shells corresponds to an equivalent position in the 2D plane strain model, meaning that the boundary conditions and displacement should also be applied in the same position to obtain comparable results between the two models. See Figure 3.8 for details.

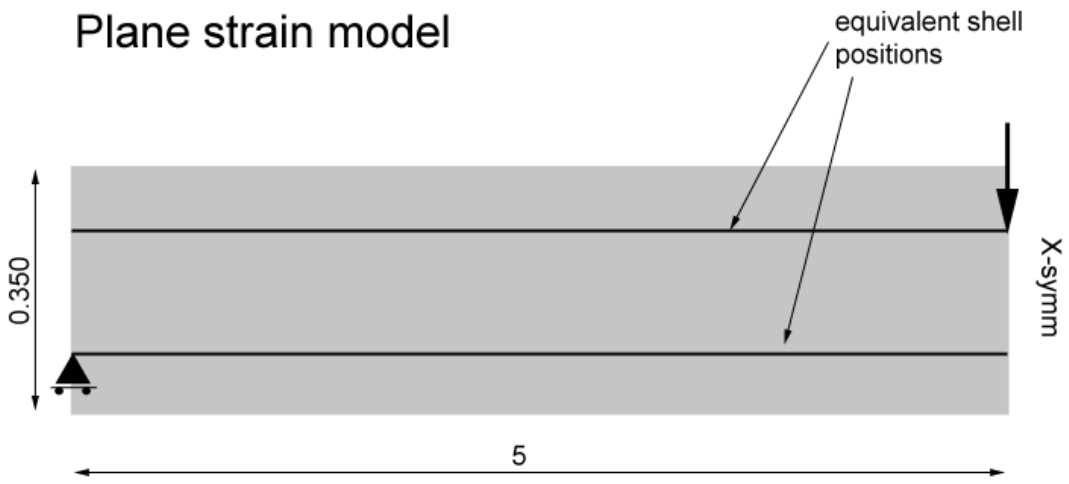

Figure 3.8 – Plane strain and conventional shell model

Another consideration is that the "plane strain" boundary conditions have to be set for the shell model. They shouldn't have any secondary curvature or displacements in the out-of-plane direction of the plane strain model (in the shell model corresponds to the Y-direction). Therefore for all nodes the displacement in the plane strain direction and the rotations in that plane is zero.

The support of the beam is specified by applying a zero displacement boundary condition on the respective nodes in the vertical direction, leaving the horizontal direction free to

move. Also, a punch is modeled with a radius of 0.2 mm. On the latter, a vertical displacement is applied and all the other degrees of freedom are locked. The node which is in the exact symmetry of the beam, with which the punch is in contact, is locked in the horizontal direction, to assure a purely symmetrical deformation.

Another important note is that when using symmetry, damage is not modeled the same way as it is without symmetry, because the nodes on the symmetry have double the fracture energy associated. So symmetry is only used for computing the elastic properties.

The discretization with 2D continuum plane strain, conventional shell and continuum shell elements are represented in Figure 3.9, Figure 3.10 and Figure 3.11, respectively.

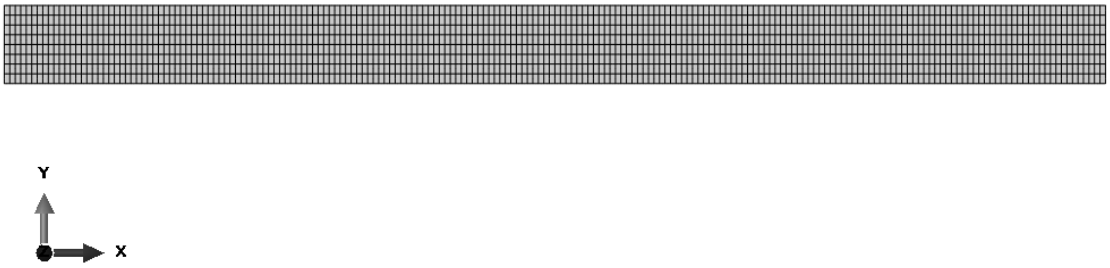

Figure 3.9 – 0/90 2D continuum plane strain (CPE8R) discretization

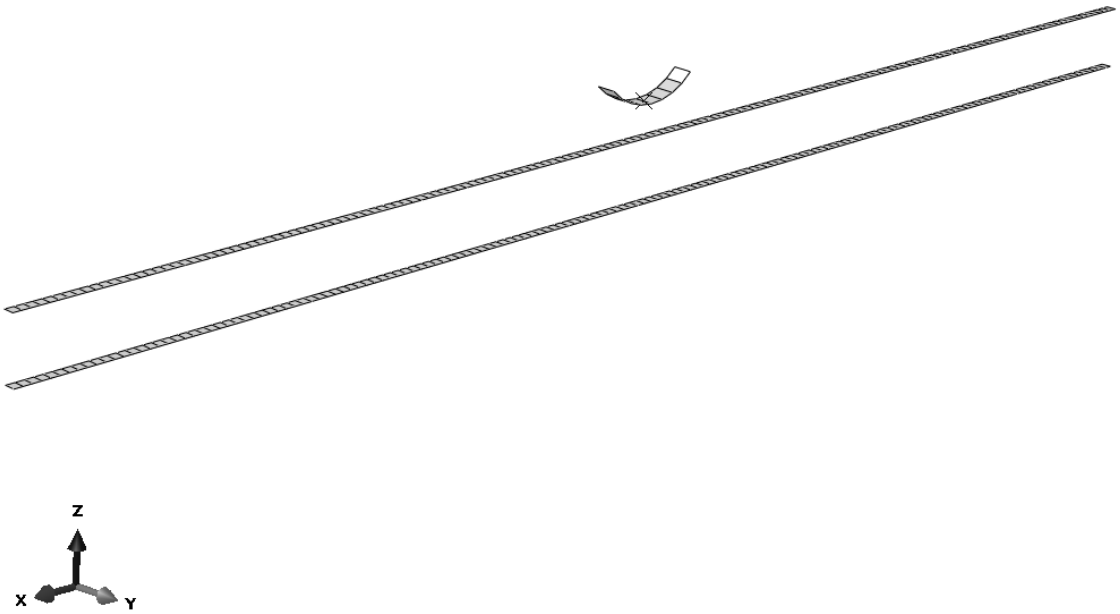

Figure 3.10 – 0/90 Conventional Shell elements (S4) discretization

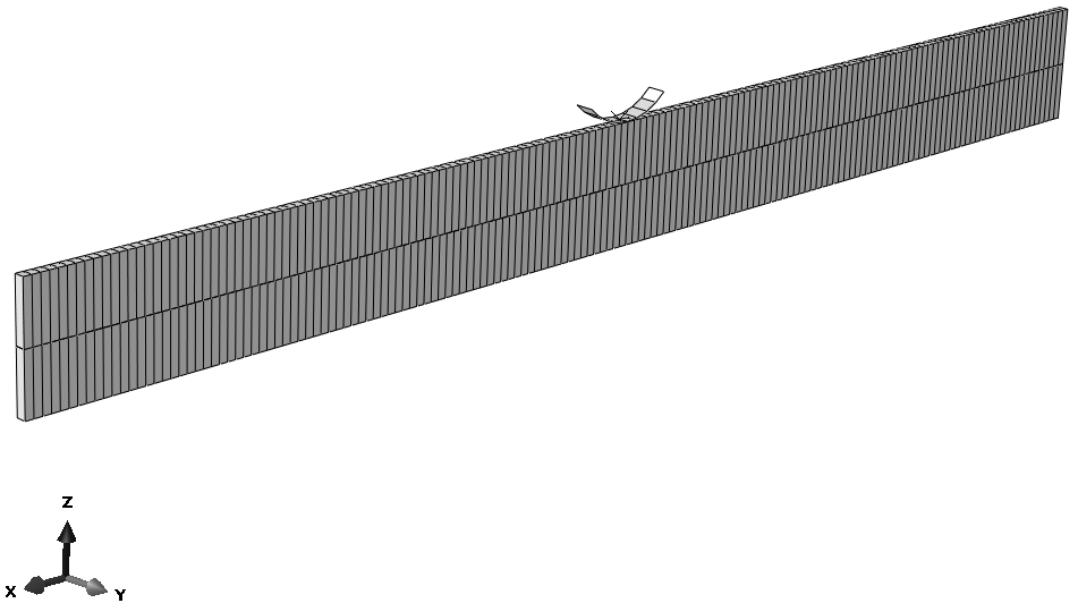

Figure 3.11 – 0/90 Continuum Shell elements (SC8R) discretization

For the continuum shells, constrain equations are defined in order to apply the boundary conditions for the supports in the middle of the ply thickness (exactly where the mid-surface would be positioned for the conventional shells) to make a more accurate comparison between the models.

For stiffness computation there are some differences in the geometrical model, such as, no punch was used and symmetry boundary conditions were applied. An element size of 0.1 was used for shell elements. Also the full beam length was used and the beam length was set by setting the boundary conditions for the support on the respective length.

3.5.2. Experimental model

Considering again a 3-point bending problem, the specimen size specification, for which guidelines are followed from EN ISO 14125 – "*Fibre-reinforced plastic composites - Determination of flexural properties*". The length of the specimen is 50 mm and 100 mm, and a width of 15 mm. The ply thickness is 0.125 mm. The radius of the punch is 5 mm. The orientations used are 0/90, where twelve plies are 0º plies and the other twelve are 90º. As well a 0/90/0/90/90/0/90/0 lay-up is considered, where each three plies have the same orientation.

The discretization is made with conventional shell elements and typically each shell layer will correspond to a different number of plies (except for the 0/90/0/90/90/0/90/0, where only an eight shell layers model is possible). A two layer model considers that each shell layer has twelve plies, a four shell layers model considers that each layer has six plies, a eight shell layers model considers that each layer has three plies and the same logic applies no matter what the number of layers is. The total amount of plies is 24 with the laminate's thickness equal to 3 mm. An element size of 0.25 is used. See Figure 3.12 for a visual representation of the eight shell layers model. The same boundary conditions are used as with the initial model and also a displacement is applied on the punch in the Z-direction.

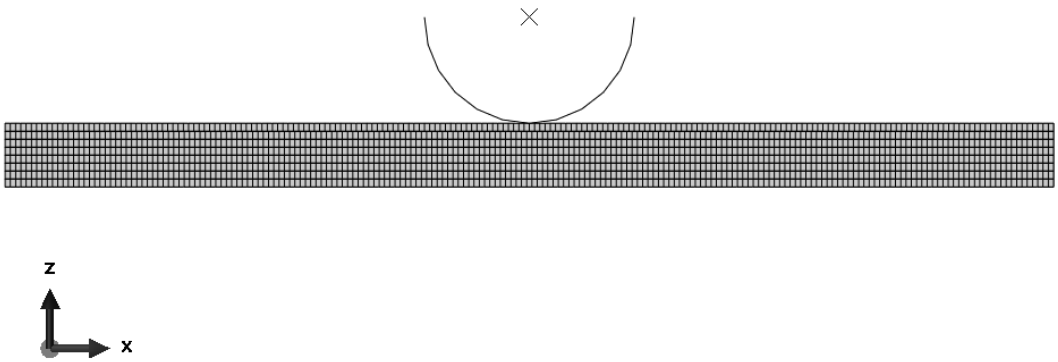

Figure 3.12 – 0/90 Eight shell layers model discretization with conventional shells (S4) with 50mm length

Another consideration within this model is that the upper layer always has an extra element comparing to the other layers, see Figure 3.13. This is chosen because the damage propagation is easier if it is done in the middle of the element and not in the node. The reason for modeling the upper layer different is thus because a zero displacement boundary condition must be applied on the node in contact with the punch in the X-direction.

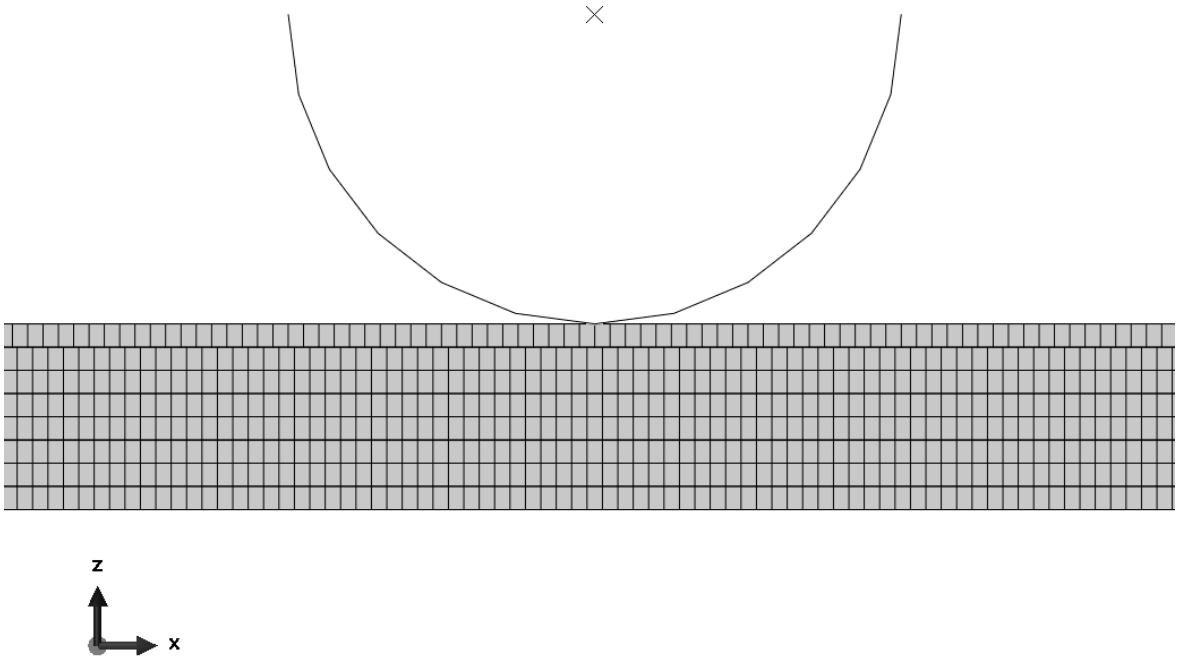

Figure 3.13 – 0/90 Eight shell layers model discretization with conventional shell elements (S4) zoomed in the middle of the beam

4. Results

4.1. Initial model results

4.1.1. Elastic properties

Table 4.1 are represents the different stiffness values obtained for different beam lengths, these values are calculated by obtaining the force from the output and dividing them by a known displacement (0.01 mm). The values serve as a comparison between different element types, as referred earlier, because with conventional shell elements with a cohesive surface the stiffness is overestimated [16]. Also it is interesting to know if the stiffness is overestimated because of the cohesive surface, so a composite section is also used, this refers to the one layer models. In fact, the one layer models do not have much use, as the interface is not damageable, but in this case we are dealing with linear elastic simulations. What can be concluded is that for the conventional shell elements the stiffness is only overestimated when using a cohesive surface. Such influence cannot be found on other element types. Even so, this conclusion is valid only for small length-to-thickness ratios, where the effect of transverse shear is higher, then the difference in stiffness becomes particularly large between them. The difference in stiffness between the Euler and Timoshenko beam is a good comparison of the amount of transverse shear, if the difference between them is insignificant, then the transverse shear is negligible. In order to figure out the reason of the overestimated transverse shear stiffness attempts were made within simpler models. An isotropic beam was used with a cohesive surface and two shell layers. Also, a one element model was used, with pure bending and pure transverse shear load cases. In the end, the results were inconclusive.

Stiffness for 0/90 model	Beam length / length-to-thickness ratio		
	1mm / 2.86	4mm / 11.4	10mm / 28.6
Conventional shell 1 layer	66.16	2.251	0.1639
Conventional shell 2 layers	115.9	2.362	0.1653
Continuum shell 1 layer	44.16	2.183	0.1632
Continuum shell 2 layer	53.36	2.210	0.1634
2D continuum (plane strain)	64.44	2.884	0.2013
2D continuum (plane stress)	54.50	2.350	0.1626
Timoshenko beam	70.13	2.379	0.1629
Euler beam	165.1	2.580	0.1651

Table 4.1 – Stiffness values in MPa for different element types and beam lengths for the 0/90 beam

Another consideration regarding the results in Table 4.1 is the overestimated stiffness with the 2D continuum plane strain elements. Especially, the value for the 10 mm beam that has an approximate error of 20% when compared with the other models or with the analytical solution. The difference arises from the implicit plane stress assumption of classical beam theory. Naturally, the zero strain will make the beam stiffer. The same simulations were done with 2D continuum quadratic elements in plane stress with reduced integration (CPS8R) and the results fit better with the other element types and the analytical solution, at least, for the 10mm beam.

For future considerations it may be interesting to see what will happen with the transverse shear when more than one cohesive surface is used.

4.1.2. Damage modeling

In this section, a comparison between continuum shell elements and conventional shell elements is provided. From the thesis [16] there is a lot of description of damage modeling with conventional shell elements, but no information on continuum shell elements was provided. These elements are known to provide good results with load cases where the contribution from transverse shear is high [1] and, as seen in the section above, they are better with the initial stiffness. But with damage modeling this is not the case, as the transverse shear stresses or strains are not included in the damage model and failure occurs due to bending. For the latter, these elements are not the most adequate, as they have no rotational degrees of freedom and they are bilinear elements. Additionally, they are susceptible to "hourglassing". These results are evident on the force-displacement graphs on Figure 4.1, Figure 4.2 and Figure 4.3 for the 1 mm, 4 mm and 10 mm beams, respectively. Their length-to-thickness ratio is represented in the preceding section in Table 4.1. Also, what can be observed is that the difference in initial stiffness becomes larger as the contribution from the transverse shear increases.

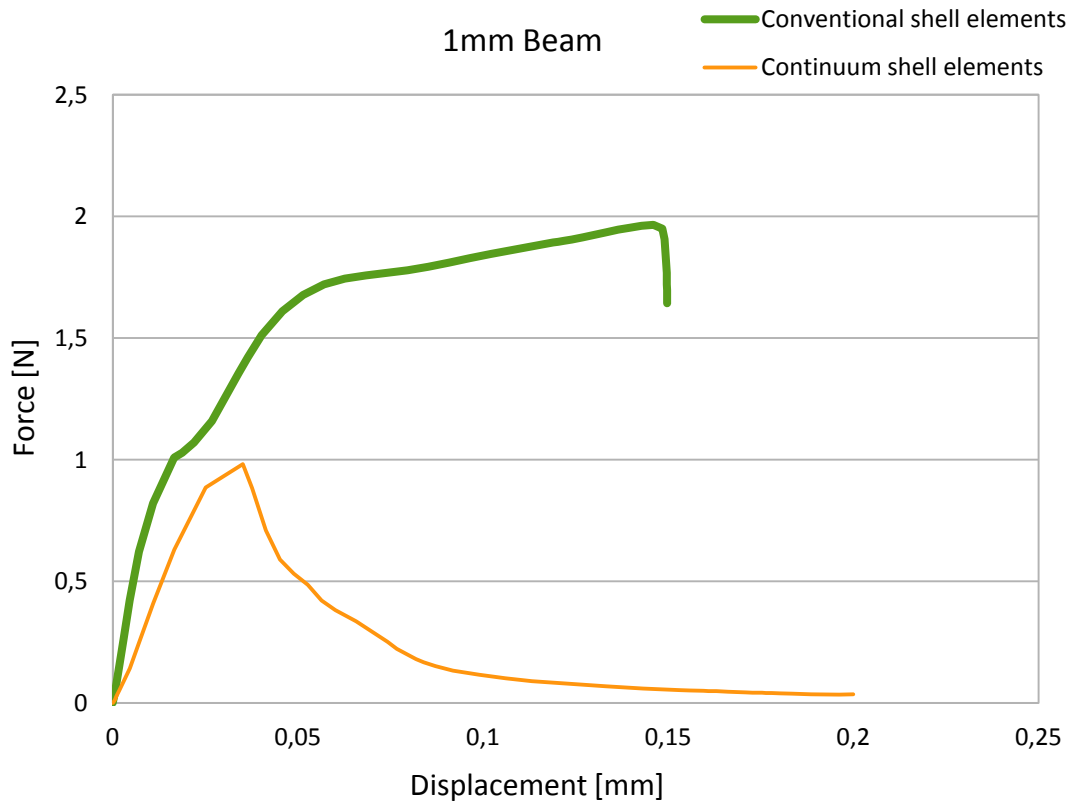

Figure 4.1 – Force-displacement plots represented for the 0/90 continuum shell and conventional shell models with two layers and a cohesive surface for the 1mm beam

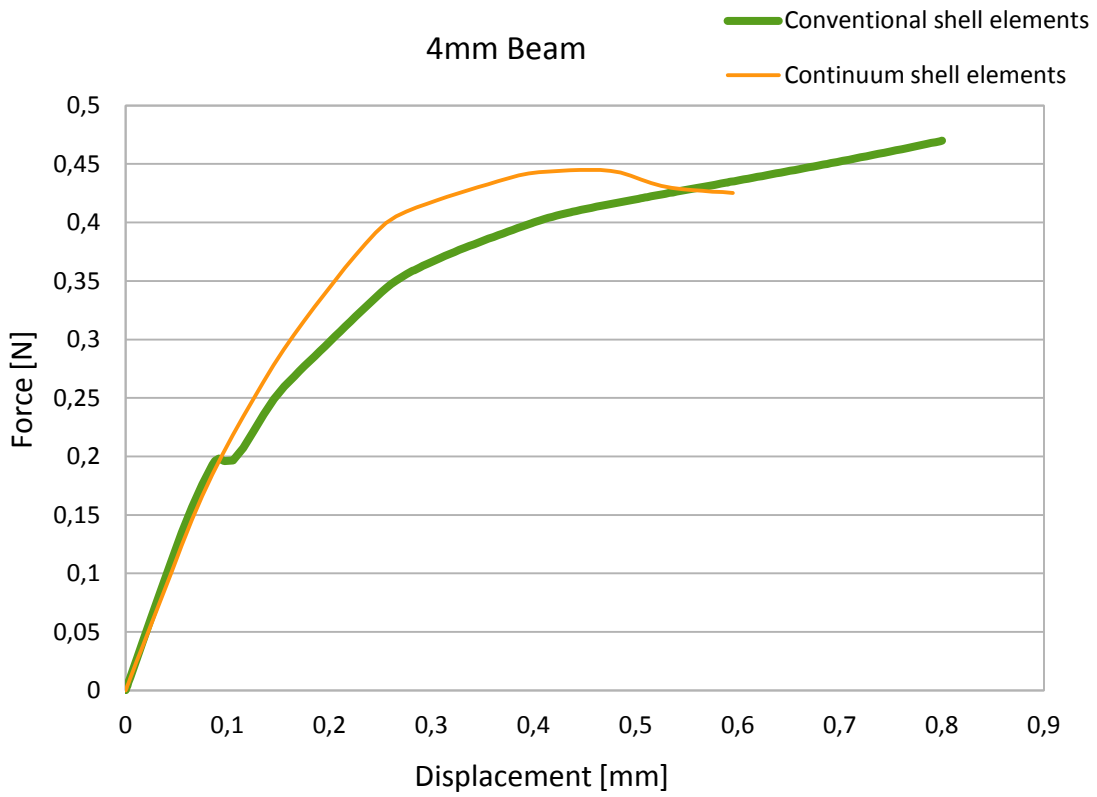

Figure 4.2 – Force-displacement plots represented for the 0/90 continuum shell and conventional shell models with two layers and a cohesive surface for the 4mm beam

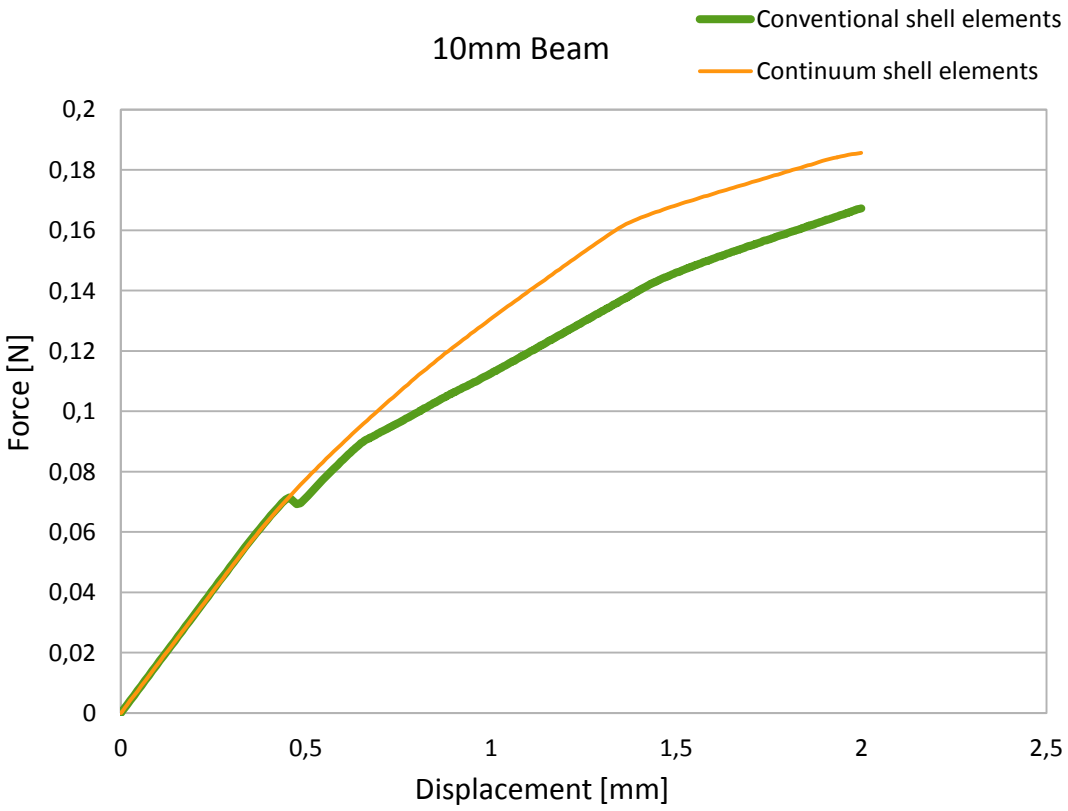

Figure 4.3 – Force-displacement plots represented for the 0/90 continuum shell and conventional shell models with two layers and a cohesive surface for the 10mm beam

From the analysis of the plots above it can be observed that there is a structural softening. It occurs in the region where the tangent stiffness matrix has negatives values. Such softening occurs after FPF with the conventional shell element models. The exception holds for the 1 mm beam model where the specimen size is rather small. When the specimen size increases the structural softening region increases as well, as the amount of fracture energy is also higher. On the experimental model, further in this thesis, this will be clearer. For all the beam lengths, the conventional shell models fails through the lower layer with matrix tensile damage growing until the interface and then delamination.

Such a structural softening normally occurs with delamination, but it cannot be observed with continuum shell elements. The softening observed in the case of the 4 mm beam is rather more common to single ply failure, with high non-linearity in the beginning and softening in the end. In any case, damage initiation of the interface can be observed, but no visible opening (Figure 4.4).

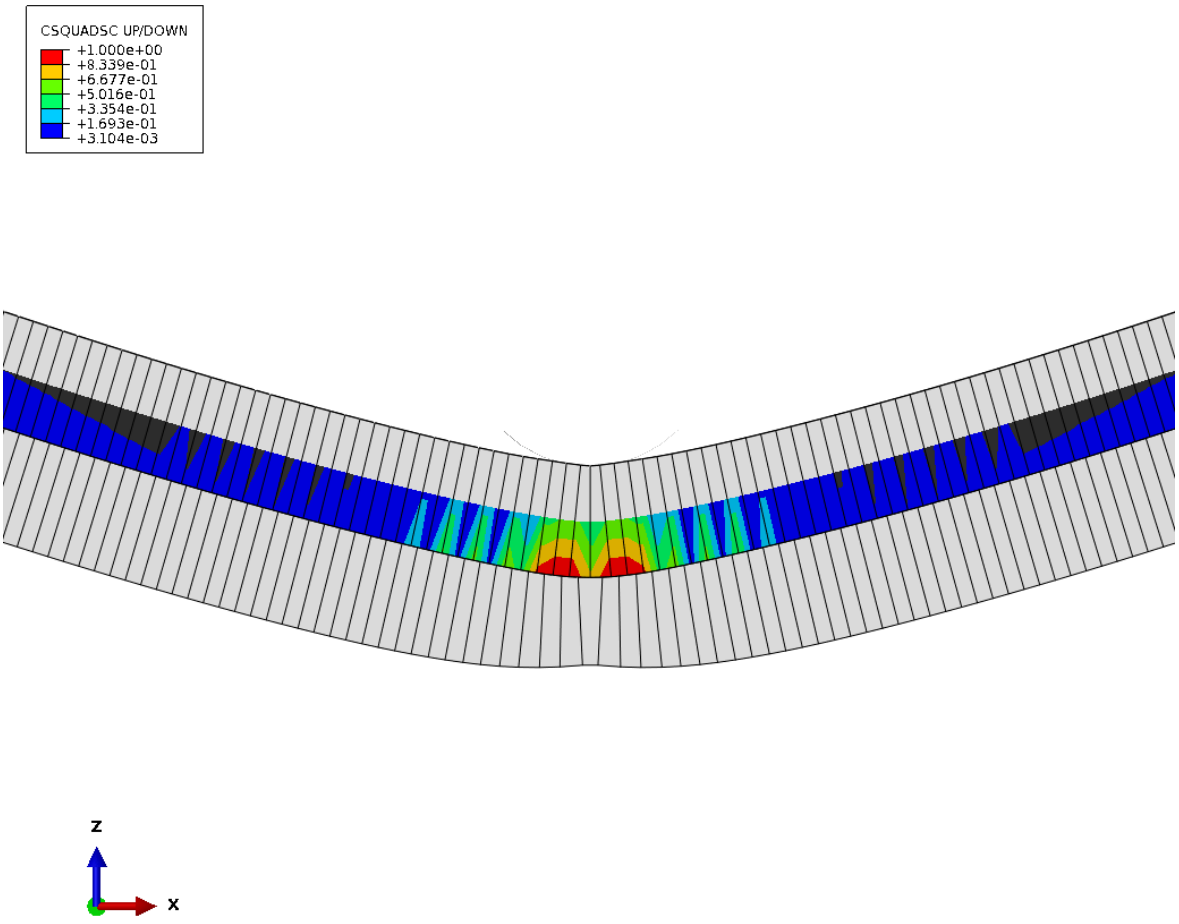

Figure 4.4 – Interface damage initiation criterion represented on the lower layer for the 0/90 continuum shell model with two layers and a cohesive surface. (*F* = 0.4251 N, *w* = 0.5951 mm)

As for the crack growth (with matrix tensile damage) through the 90º layer ply, it is not in the center of the beam as expected (Figure 4.5). This could be due to "hourglassing" and symmetric thickness reduction in the center of the beam (Figure 4.6). Continuum shell elements are susceptible to "hourglassing" as they use reduced integration.

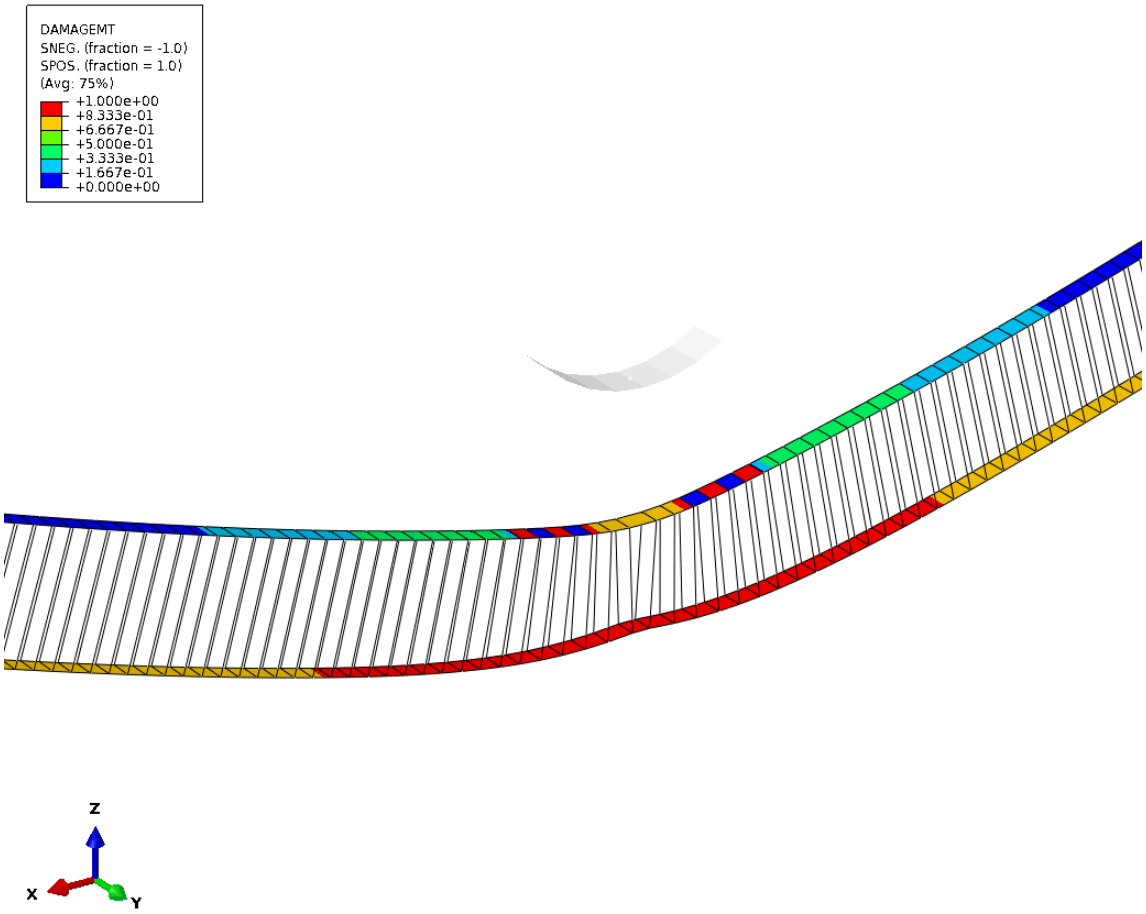

Figure 4.5 – Matrix tensile damage represented on the lower layer for the 0/90 continuum shell model with two layers and a cohesive surface. The upper layer is hidden for better observation. (*F* = 0.4251 N, *w* = 0.5951 mm)

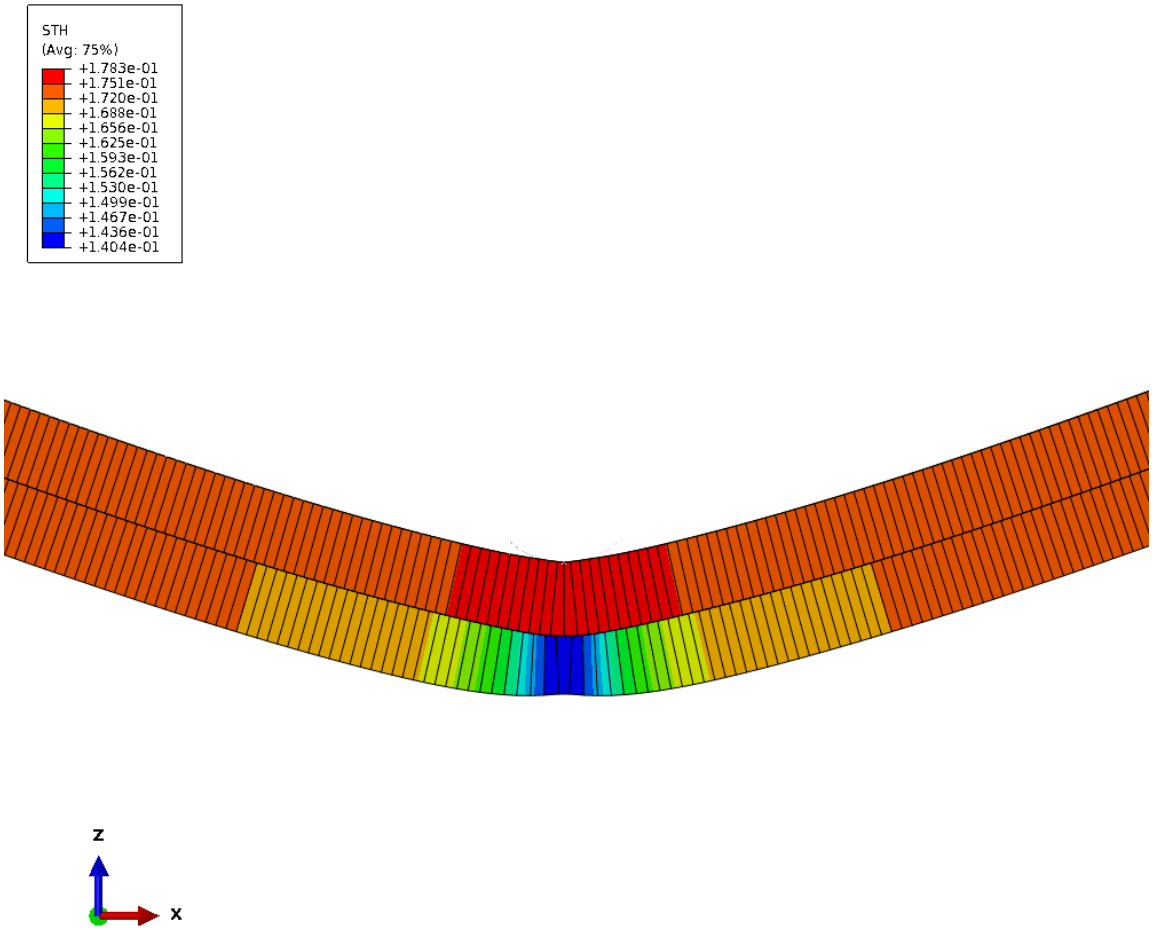

Figure 4.6 – Thickness variation represented on the lower layer for the 0/90 continuum shell model with two layers and a cohesive surface. (*F* = 0.4251 N, *w* = 0.5951 mm)

With continuum shell elements, in the case of the 10 mm beam there is no softening. The exception holds for the 1 mm continuum shell beam, which in any case, fails on the supports and not in the middle of the beam (as with conventional shell model, with failure on the element in the center of the beam on the lower layer). It would be unlikely that delamination would occur at a free edge. A comparison between the conventional and continuum shell models with visible delamination of the 1 mm beam can be made based on Figures 4.7 and 4.8.

As seen in Figure 4.8 it is important to refer that the thickness represented by the conventional shells is only a post processing expansion of the shell mid-surface. But it is also important to refer that in the post processing the rotational degrees of freedom are not represented. This expansion was only used to make delamination visible with an opening between the two shell layers.

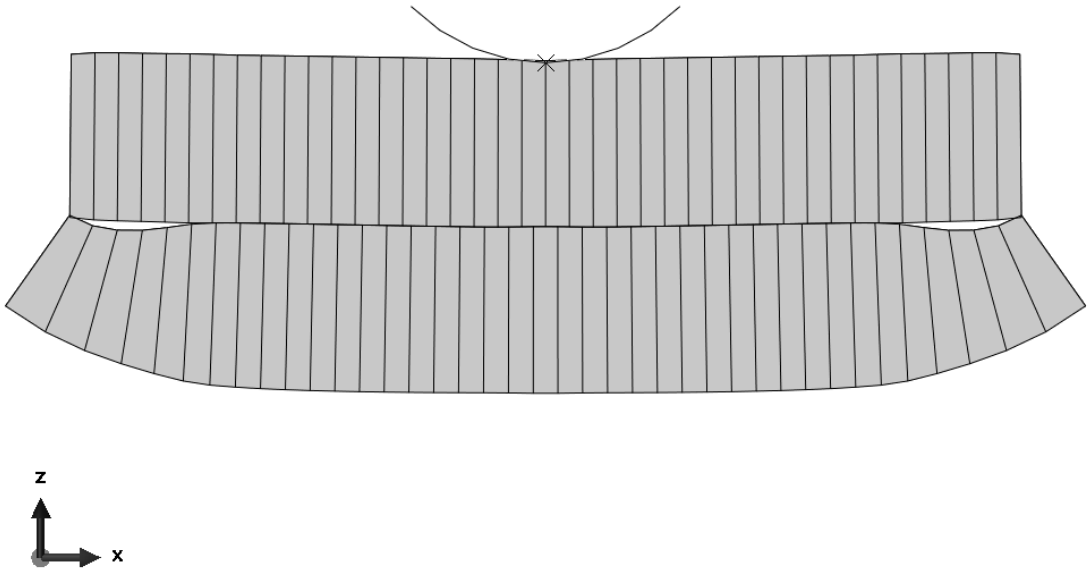

Figure 4.7 – Continuum Shell model for 1mm beam, with failure on the supports and delamination

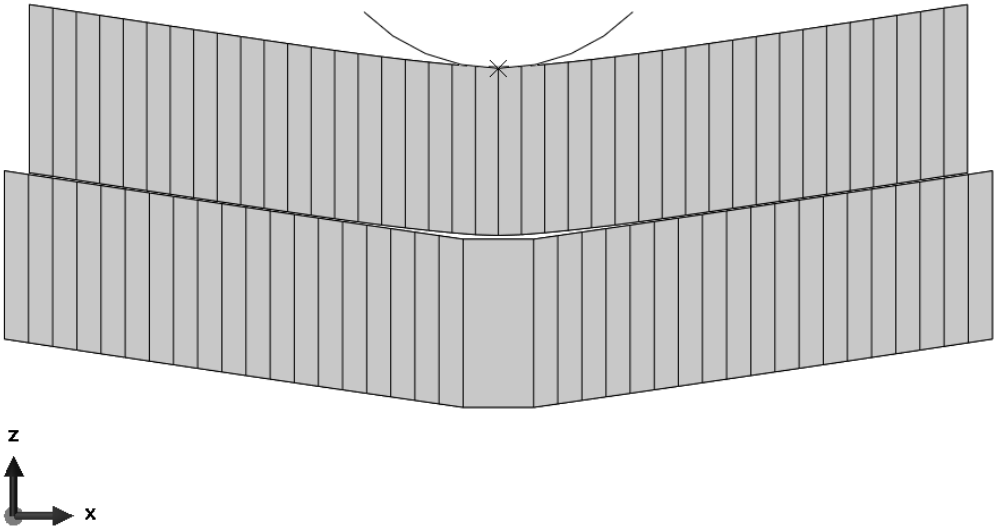

Figure 4.8 – Conventional Shell model for 1mm beam, with failure in the element in the middle of the beam and delamination

On the final conclusions made on the continuum shell elements, the results obtained are not trustable, due to "hourglassing", symmetric reduction of thickness, no crack growth through the center of the beam (where the bending stresses are expected to be maximum) and no structural softening after FPF. Therefore, for the next section of the thesis, where are the results for the experimental model, only conventional shell elements will be used.

4.2. Experimental model results

In this section, the modeling results are presented for the future experiment. The focus of study in this section is the influence of different contact formulations. As referred already, the behavior will be different depending on which surface is defined as master or slave. This is a flaw of ABAQUS. Also, the surface-to-surface or node-to-surface will provide different results as contact pressures between the shell layers are calculated with different contact formulations. Changed interface strength and toughness are applied, which will be discussed in more detail in the sections below. Finally, it is also interesting to investigate the difference in the behavior by using a different number of layers. These comparisons will provide useful information for the analysis of experiment data, as some computations will be more accurate and others less accurate. The structure of the results in this section is explained in Table 4.2, where the configurations that have been computed are marked by crossess. Typically, but with some exceptions, the results will be presented by force-displacement plots grouped together by rows or columns from the table.

Configuration / Ply lay-up		0º as master		90º as master	
		Normal interface values	Changed interface values	Normal interface values	Changed interface values
Surface to Surface	0/90 2-layer	✗		✗	
	0/90 4-layer	✗	✗	✗	✗
	0/90 8-layer	✗	✗	✗	✗
	0/90 12-layer			✗	✗
	0/90 16-layer			✗	✗
	0/90 24-layer			✗	
	$[0/90/0/90]_S$ 8-layer	✗		✗	
Node to Surface	0/90 2-layer	✗		✗	
	0/90 4-layer	✗	✗	✗	✗
	0/90 8-layer	✗	✗	✗	✗
	0/90 12-layer			✗	✗
	0/90 16-layer			✗	✗
	0/90 24-layer			✗	
	$[0/90/0/90]_S$ 8-layer	✗		✗	

Table 4.2 – Simulations for the experiment model

4.2.1. The reference eight layers 0/90 model

The presentation of the results starts with the eight shell layer model, as it is the reference model. The other models will be presented in the following sections. Figure 4.9 represents the force displacement dependence. The sequence of events for damage initiation and damage evolution are as well marked on the graph, which follows what was initially expected and already seen with the initial model, with conventional shell elements. Marking the sequence of events is important for characterizing the behavior of a laminate. Where the matrix tensile damage initiates corresponds exactly to FPF. The simulation before FPF is linear, as the non-linearity occurs due to stiffness degradation with damage evolution. What happens afterwards is the matrix tensile failure, which is characterized by a crack growth through the thickness. This means that ply failure has only occurred after the elements in the center of the beam in the 90º layers, through the thickness have the matrix tensile damage evolution criterion equal to one. Then naturally the damage will start on the interface and again failure is considered only when the damage evolution criterion for the interface is one.

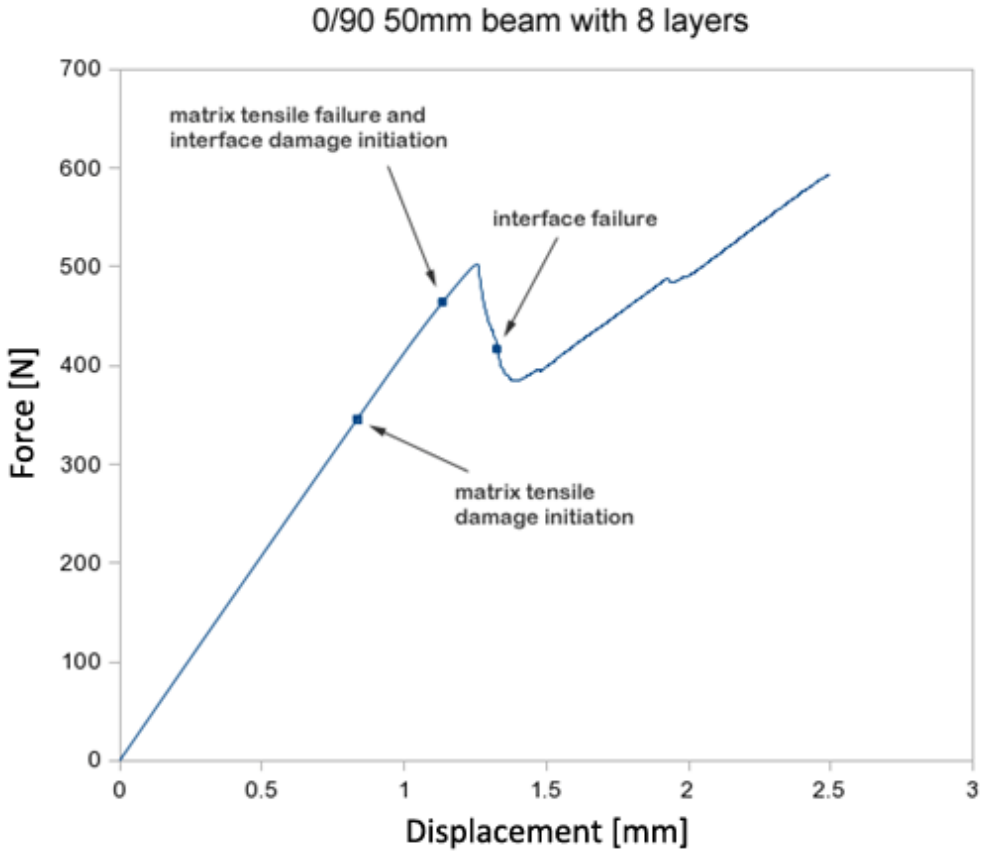

Figure 4.9 – Force-displacement graph of the eight shell layers 0/90 model with surface-to-surface formulation and the lower layers defined as master surface

Even though the loads and displacements are well marked on the force-displacement plots, it is always useful to take a look at the damage distribution throughout the model (Figure 4.10). In this case we have a visible delamination at two interfaces. The first delamination occurs between the two 90º/90º layers, then the damage spreads to the sides creating a second delamination between the two 0º/90º layers. As discussed further in this Chapter all simulations will typically delaminate only between the 0º/90º layers, even so it does not mean that this result is less correct.

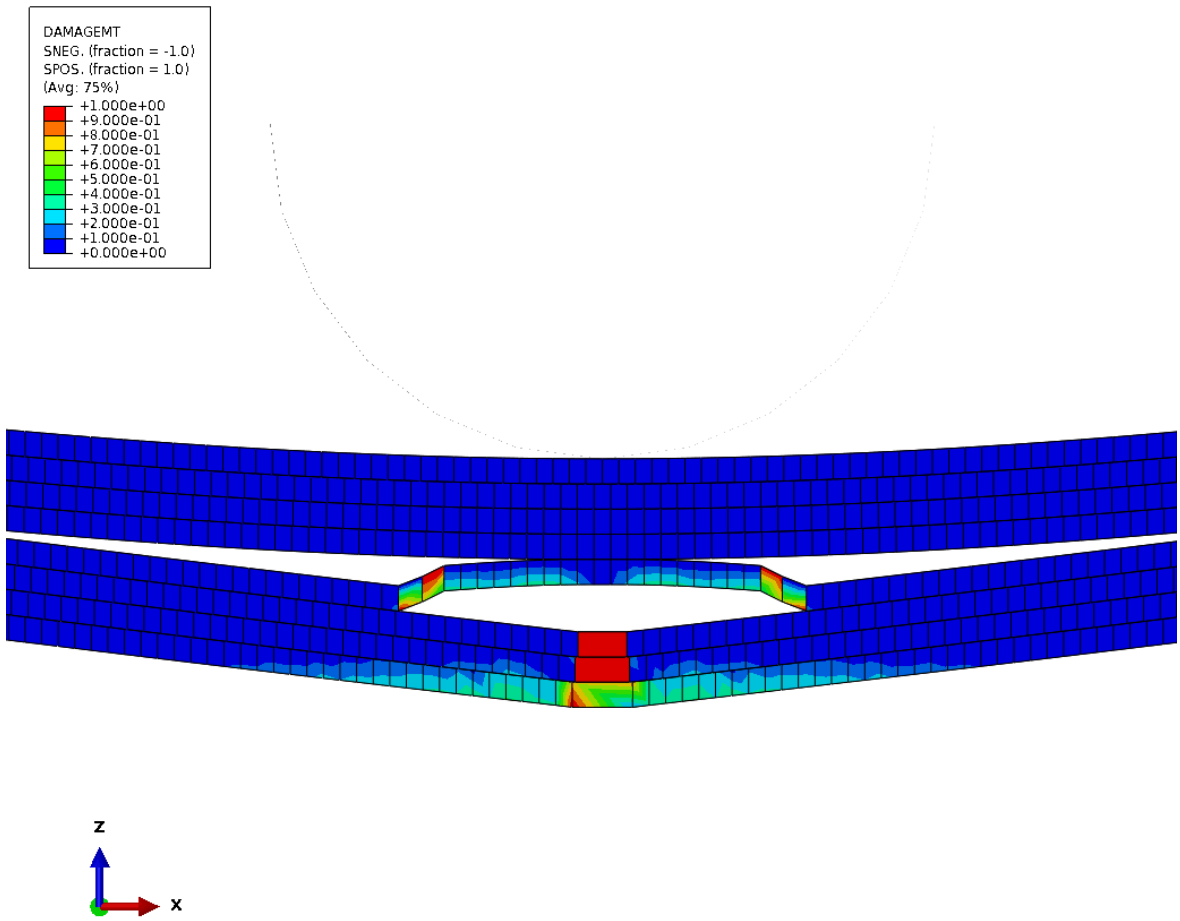

Figure 4.10 – Delamination (visible opening) and matrix tensile damage (color contours). 0/90 eight shell layers model with surface-to-surface formulation and the lower layers defined as master. (*F* = 593 N, *w* = 2.5 mm)

From the eight shell layers model the results appear to be reasonable, but further simulations with other configurations are interesting to have more information on different modeling strategies.

4.2.3. Influence of curing stresses

During the manufacturing of laminates, thermal stresses are introduced, and these tend to decrease the strength of the structure. This occurs due to different expansion factors for different directions. When the laminate is constrained it cannot expand, then residual stresses remain afterwards. To account for this, an initial temperature of 177 ºC is set and in an additional step another temperature of 20 ºC is applied. Orthotropic thermal expansion coefficients are defined in the material data as $\alpha_{ll} = 1e^{-06}$, $\alpha_{qq} = 1.8e^{-05}$ and $\alpha_{tt} = 1.8e^{-05}$ [1/ºC].

In Figure 4.9 a force-displacement graph represents the influence of curing stresses within the model described above. The displacement does not assume negative values, because during the step where thermal stresses are introduced, the punch has a zero displacement, not allowing the laminate to expand. The effect of the curing stresses on the strength is quite large, but afterwards both force-displacement plots follow the same path.

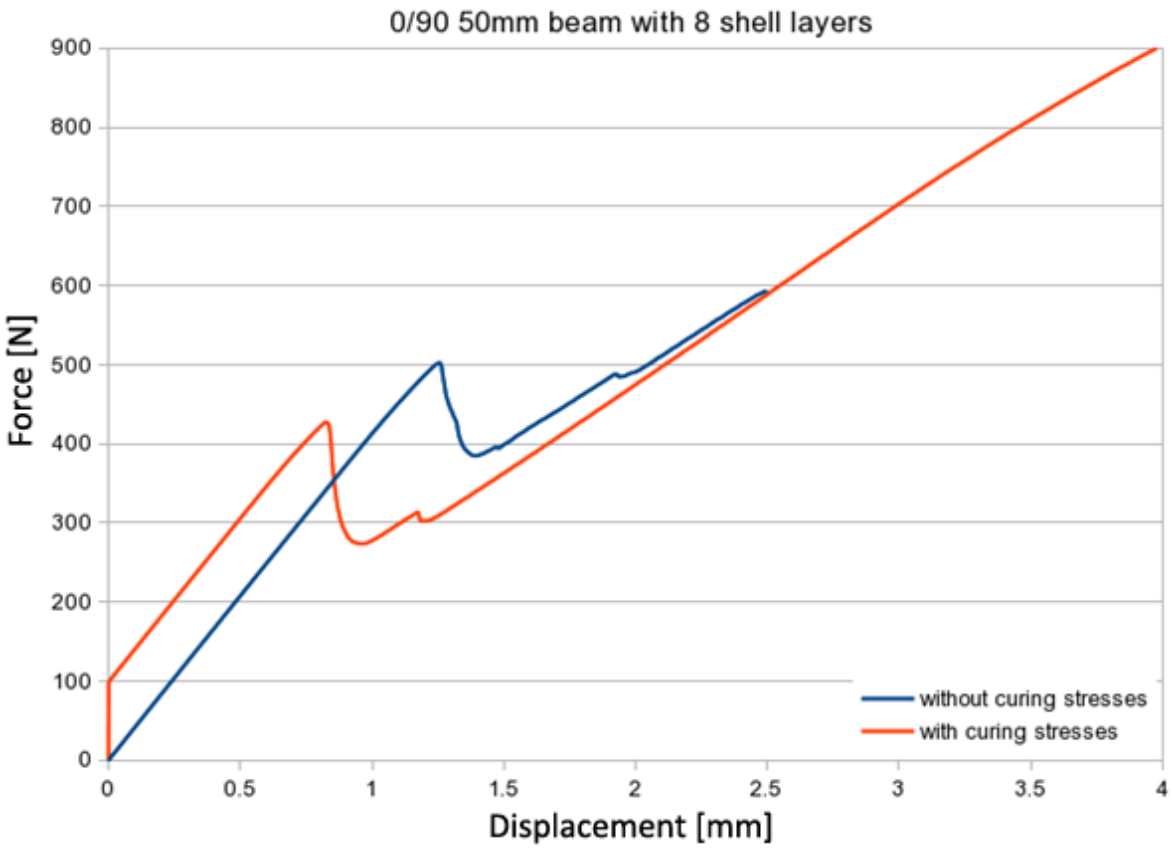

Figure 4.11 – Force-displacement graph showing influence of curing stresses with the 0/90 eight shell layers model with surface-to-surface formulation and the lower layers defined as master

Another influence of the curing stresses is that delamination occurs only between the 0º and 90º layers, in contrast to that without curing stresses (Figure 4.8).

4.2.3. Influence of the number of shell layers

In this section the influence of the number of shell layers is investigated for the same specimen. The latter possesses 24 plies with each ply thickness of 0.125 mm. In the modeling approach, different number of plies per layer are experimented in order to figure out if there is a effect of the number of shell layers modeled, because the same specimen can be modeled with a different number of shell layers. The difference is due to the fact that increasing the number of layers imply also an increased number of interfaces. In theory this should not affect damage modeling as the total fracture energy is dependent on the element size. But this is not the case, because damage tends to spread out through the ply instead of through the thickness with an increasing number of layers.

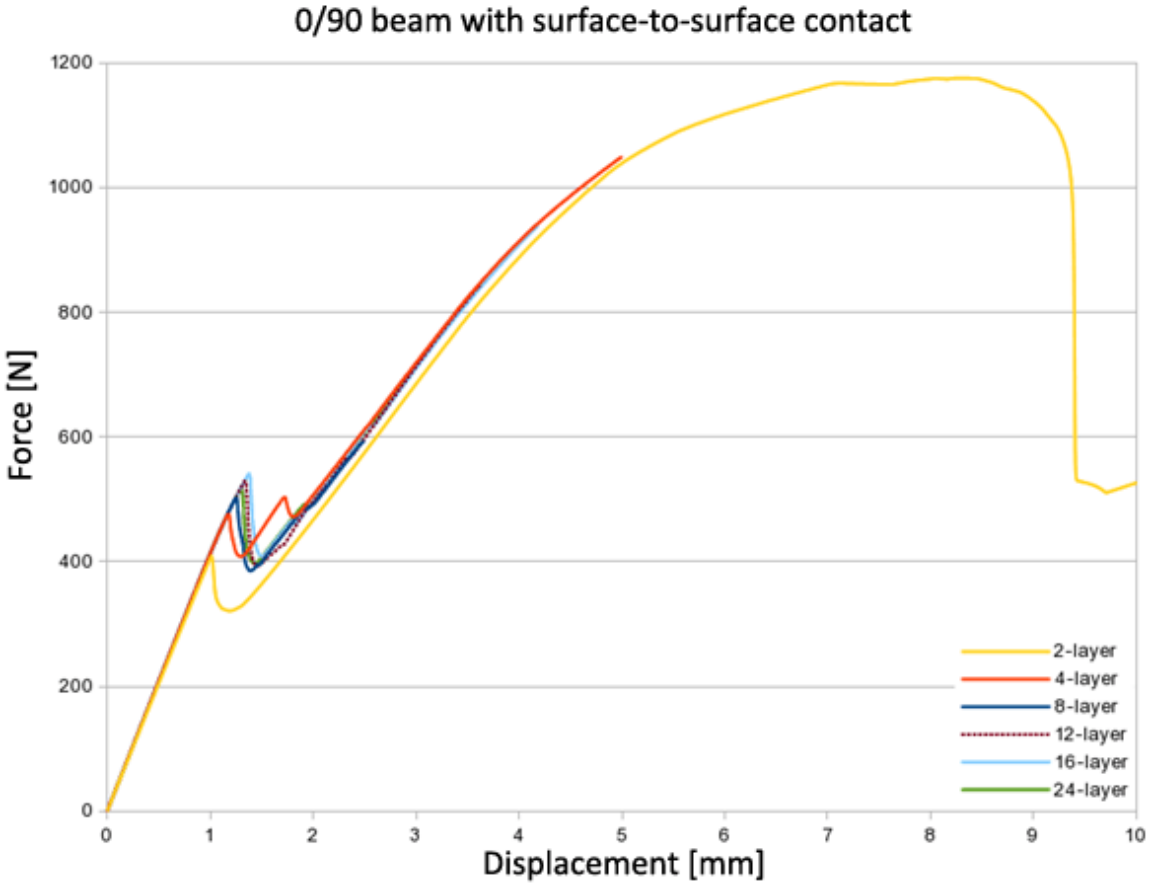

Figure 4.12 – Force-displacement graph with different numbers of shell layers for the 0/90 beam with surface-to-surface formulation and the lower layers defined as master

The reference eight shell layers model with three plies per layer is compared to the two, four, 12, 16 and 24 shell layers models in a force-displacement graph shown in Figure 4.12. What is important to note here as well is that the 16-layer does not correspond to a real amount of plies (every shell layer corresponds to 1.5 plies). However it is useful for the understanding of the effect of the number of shell layers on damage modeling.

It can be observed in this Figure that just the two shell layers model converged until the failure of the whole structure, nevertheless all the models converge until the structural softening along with delamination, see Figure 4.13 for details. The final failure of the structure is dependent on the 0º orientation shell layers, as after the structural softening the 90º orientation shell layers have already failed. It can be assumed that convergence until the final failure of the structure is easier with the two layer model, because there is only one 0º orientation layer, while other models have more and have to deal with the interfaces in between as well.

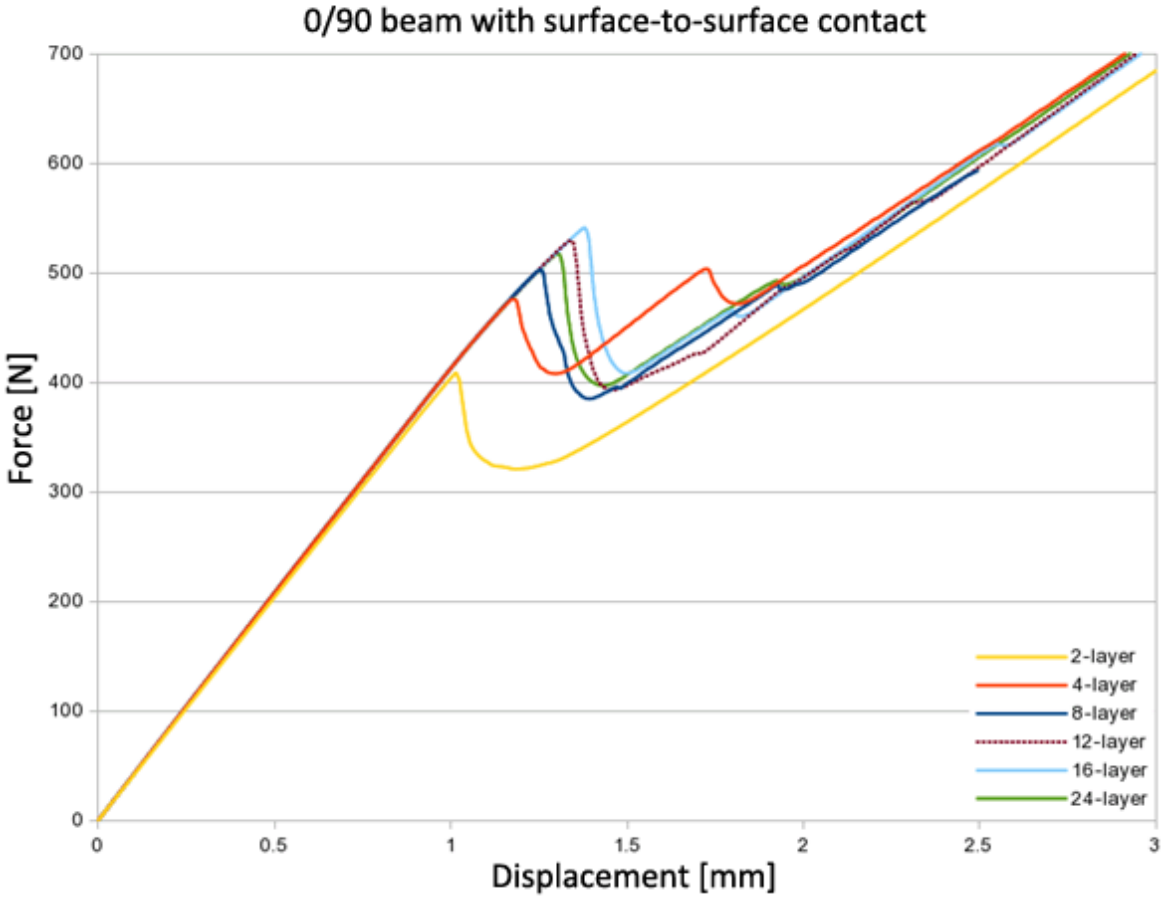

Figure 4.13 – Softening region zoom up of Figure 4.12

In Figure 4.13 it can be observed that as the number of layers increases, the strength increases as well. The exception holds for the 24-layer model, which has an intermediate strength between the eight layer model and the twelve layer model. In fact, this is a positive result, as it could mean that the strength is not proportionally increasing with the number of layers, but further simulations should be made with more layers to confirm the tendency.

As already mentioned the increase in the strength, could be related to a bigger number of interfaces, which affects the damage distribution. In order to confirm this, Figure 4.14 shows the damage distribution in the 16 shell layers model and Figure 4.10 presents the damage distribution in the eight shell layers model. With more layers, the damage is more spread out inside the shell layer, and this could be caused by the additional interfaces.

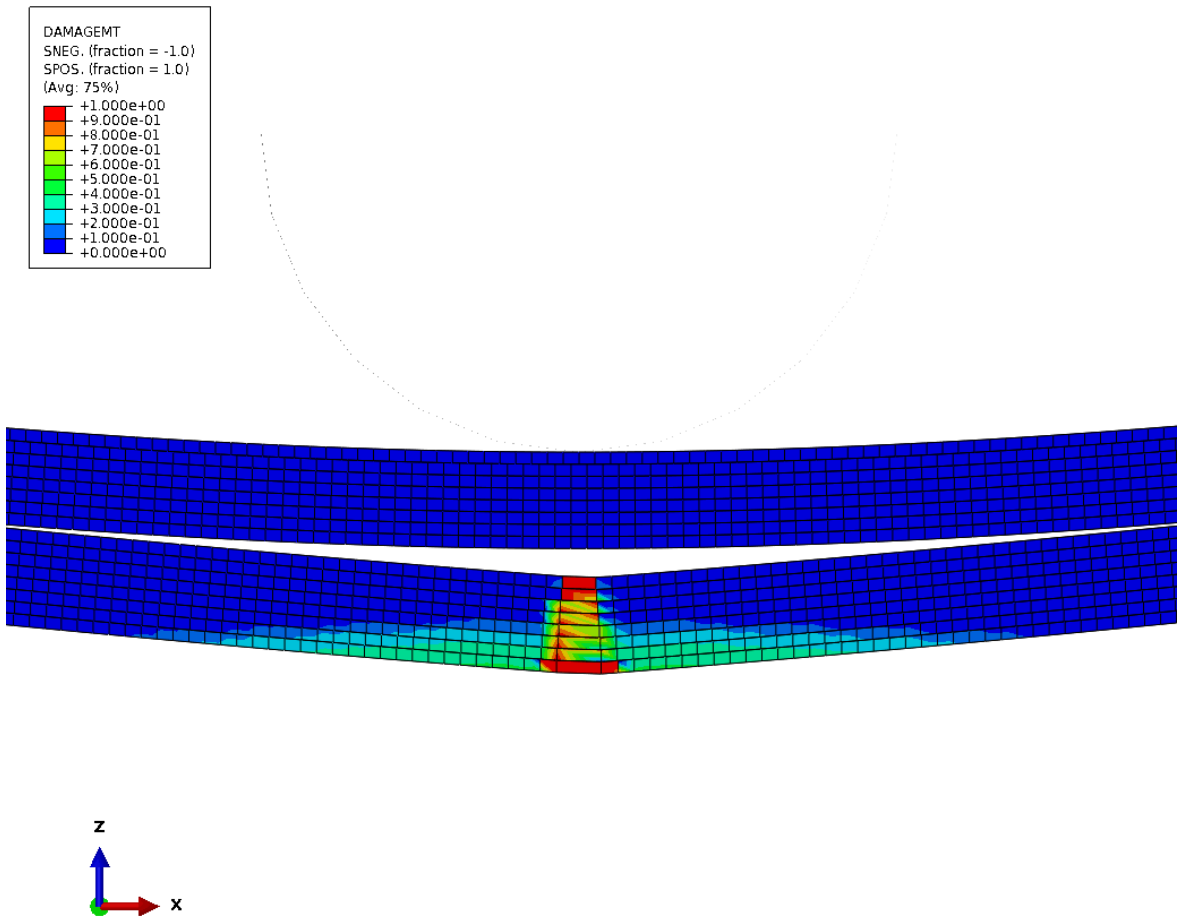

Figure 4.14 – Delamination (visible opening) and matrix tensile damage (color contours) of the 0/90 16 shell layers model with surface-to-surface formulation and the lower layers defined as master. (*F* = 608 N, *w* = 2.5 mm)

4.2.4. Influence of the variation of interface parameters

This section presents results in a similar structure as set in the previous section, except of using increased strength and toughness values for the interfaces between shell layers with the same ply orientation. Initially, identical values were used for all interfaces, but it could be that interfaces with same orientation have higher strength and toughness than those with different orientations. Therefore, average values of these are calculated between the ply transverse values and the original interface values. The new interface parameters values for the toughness and strength are represented in Table 4.3 and Table 4.4, respectively.

$\mathcal{G}_n^C$	$\mathcal{G}_s^C$	$\mathcal{G}_t^C$
0.1665	0.5746	0.5746

Table 4.3 – Changed interface fracture energy rates in J/m^2

t_n^0	t_s^0	t_t^0
71	110	110

Table 4.4 – Changed interface strengths in MPa

In Table 4.4 only the normal value for the strength t_n^0 is increased, as the shear direction values already correspond to the ply material strength.

The force-displacement graph for the changed interface values can be seen in Figure 4.15, with a zoom up on the softening region in Figure 4.16. The two shell layers model is represented only as a reference to compare the values, as it possesses no interfaces with same ply orientations, therefore the variation of the interface parameters cannot be applied to this model.

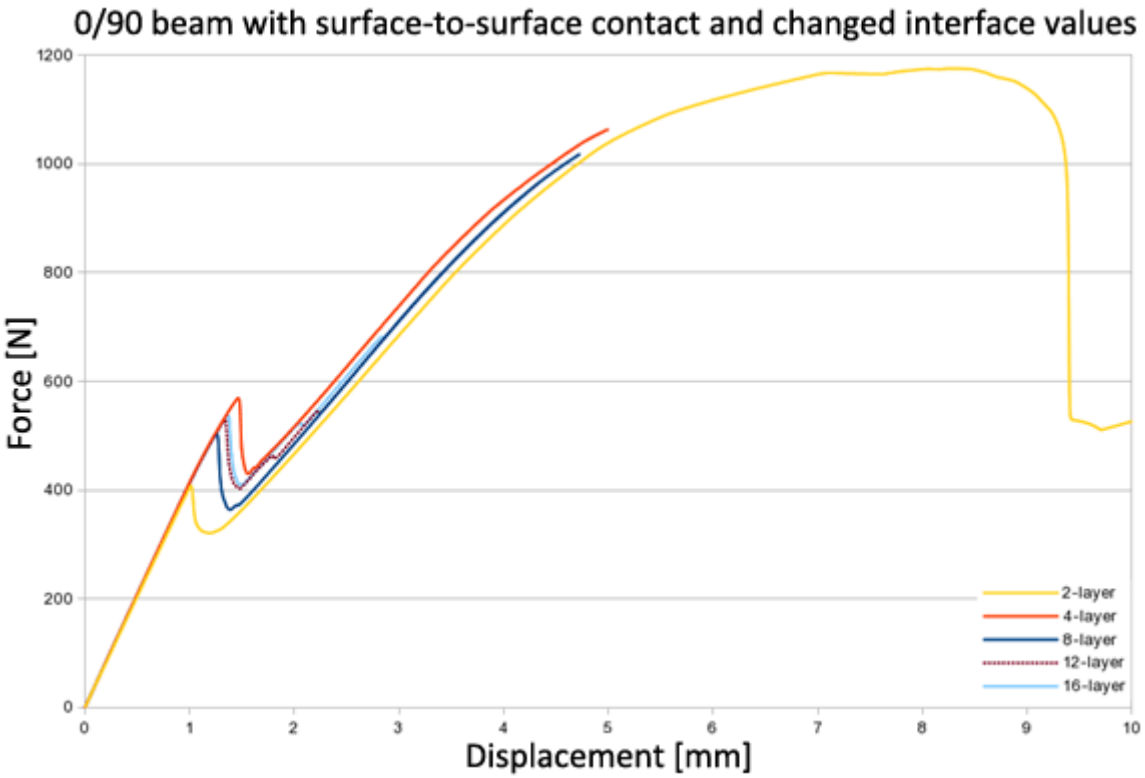

Figure 4.15 – Force-displacement graph with different numbers of shell layers for the 0/90 beam with surface-to-surface formulation, the lower layers defined as master and changed interface values

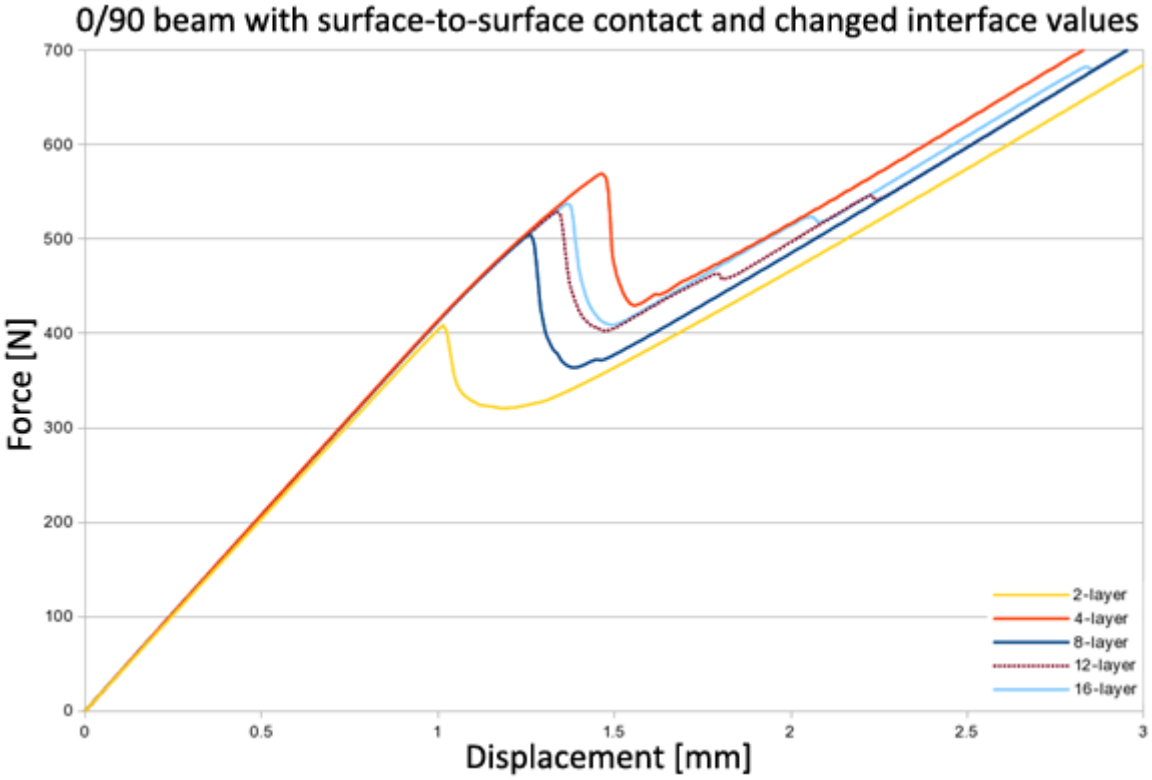

Figure 4.16 – Softening region zoom up of Figure 4.15

From Figure 4.14 it can be observed that the trend for the increasing strength with number of layers is still valid, except for the case of the four shell layers model, which will be presented in a separate category.

Figures describing damage distribution and delamination are not presented in this section, as there is not much useful information to add, except of the fact that delamination occurs just in the interface between the 0º orientation layer and the 90º orientation layer. This is explained by the lower fracture energy at these interfaces when compared to those between same orientation layers.

4.2.5. Node-to-surface contact formulation

All previous results were presented with surface-to-surface contact formulation, which are known to give more accurate results on contact pressures. Still it is interesting for the modeling strategy to establish a comparison with node-to-surface formulation.

A particular observation can be made, that node-to-surface in comparison to surface-to-surface formulation typically tends to increase the strength of all models and the strength increases as well with the number of layers. The direct comparison between surface-to-surface and node-to-surface formulation is not made in this section. This comparison can be found further in the thesis, where the two shell layers, four shell layers and eight shell layers are presented. In this section only the results concerning node-to-surface formulation are shown.

Figure 4.17 presents the different models with node-to-surface contact formulation. The two, four and eight shell layers models have a softening region, while the 12 shell layers model failure can be seen exactly before convergence ends and the 16 and 24 shell layers models do not fail. Also the final failure of the structure cannot be observed in the two shell layers, as it can be with the surface-to-surface formulation. This is expected at a relatively high displacement (20% of the beam length).

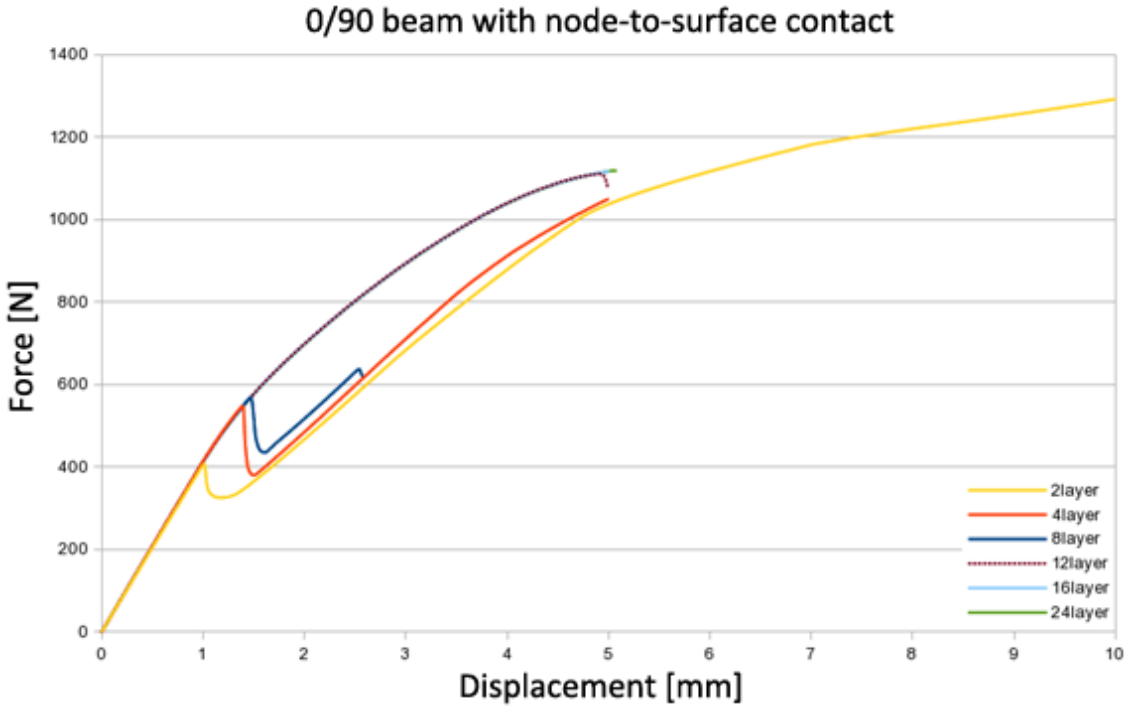

Figure 4.17 – Force-displacement graph with different numbers of shell layers for the 0/90 beam with node-to-surface formulation and the lower layers defined as master

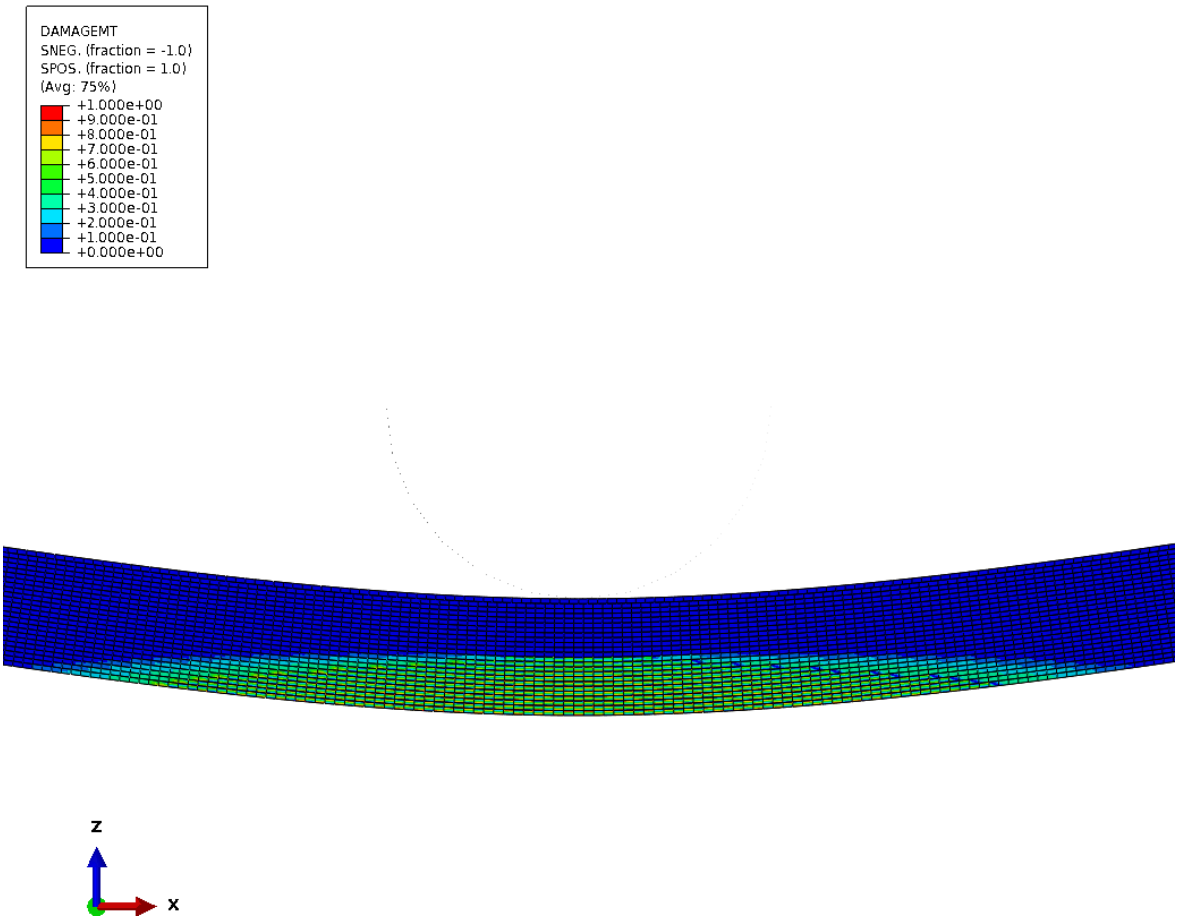

Figure 4.18 –matrix tensile damage of the 0/90 24 shell layers model with node-to-surface formulation. (*F* = 802 N, *w* = 2.5 mm)

With the increase in the strength for node-to-surface in comparison to surface-to-surface formulation the same increase can be found in the damage distribution, see Figure 4.18. This contact formulation does not provide trustable results when modeling with more than eight shell layers, because the damage corresponding to a crack growth should be localized and not spread out on the whole beam.

4.2.6. Node-to-surface contact formulation and influence of the variation of interface parameters

The results were previously interpreted with the variation of the interface values with surface-to-surface formulation. In this section the same is repeated with node-to-surface formulation.

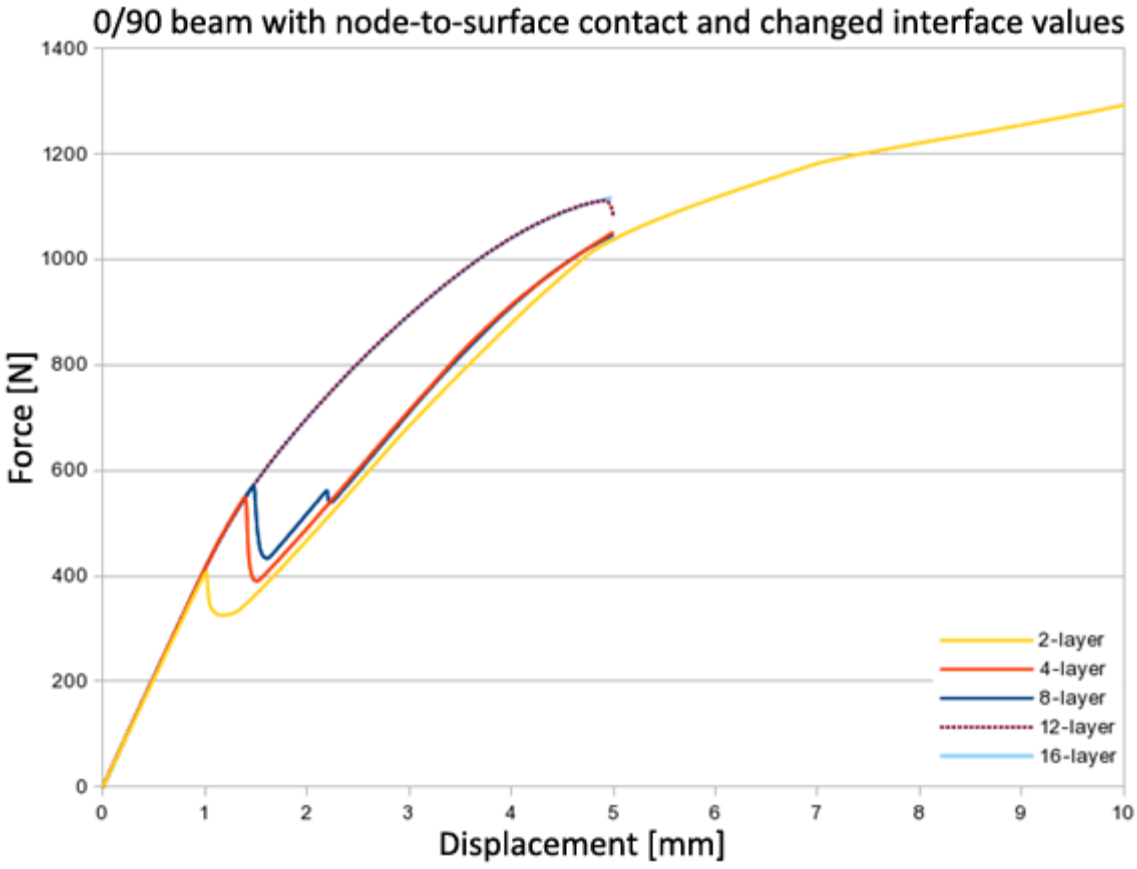

Figure 4.19 – Force-displacement graph with different numbers of shell layers for the 0/90 beam with node to surface formulation, the lower layers defined as master and changed interface values

Figure 4.19 shows the force-displacement graph with node-to-surface contact formulation and with the changed interface values, already given in the preceding section. Again, the two shell layers model is represented only as a reference to compare the values, as it possesses no interfaces with same ply orientations.

No particular observations could be made from using the normal interface values or the changed interface values in the force-displacement graphs, as the results for both are practically identical. As for the delamination the interfaces that are between layers of same orientations are naturally stronger and tougher, so they do not fail, only the interface between the 0º layer and the 90º layer. The results from this section and the section with surface-to-surface changed interface values are consistent with each other.

4.2.7. The two shell layer 0/90 model

Force-displacement plots previously presented were grouped together with different number of layers. Here the results are grouped together with same number of shell layers, but different contact formulations and master/slave surface definition. Therefore, in this section a direct comparison between switching the master/slave surfaces and between the surface-to-surface and node-to-surface formulations is made. Figure 4.20 represents the force-displacement plot for the two shell layers model.

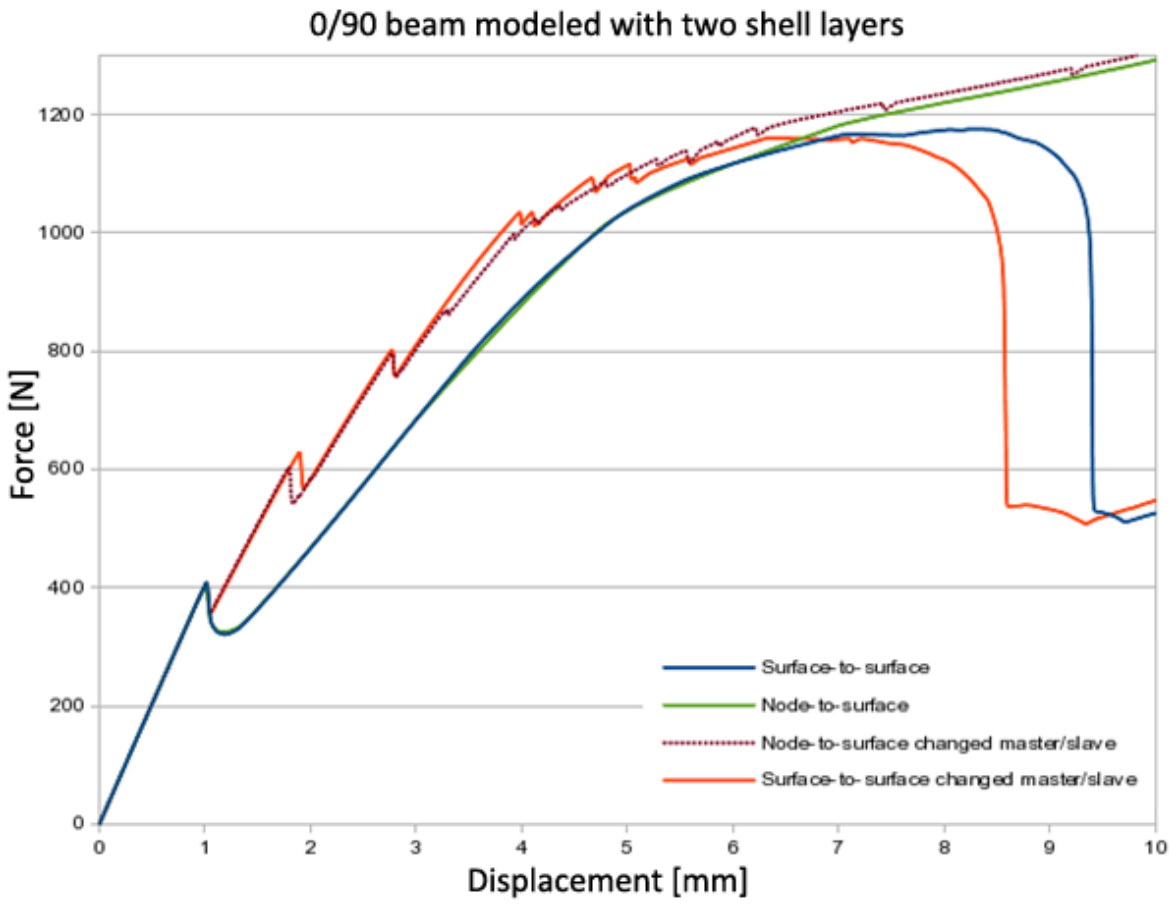

Figure 4.20 – Force-displacement graph for the 0/90 beam with two shell layers

By changing master and slave, several softening regions can be observed in this plot. This applies for both node-to-surface and surface-to-surface formulations. This occurs due to stress redistribution, in a way that more matrix tensile damage initiates in different locations, see Figure 4.21 for details. This would be the expected behavior if the interface would be perfect, which also would explain why there is no visible delamination. This is apparently a flaw of ABAQUS. It is important to remember that "normal" master/slave in the plot refers to a master surface defined at the lower layer with 90º orientation and "changed" master/slave refers to a master surface defined at the upper layer with 0º orientation.

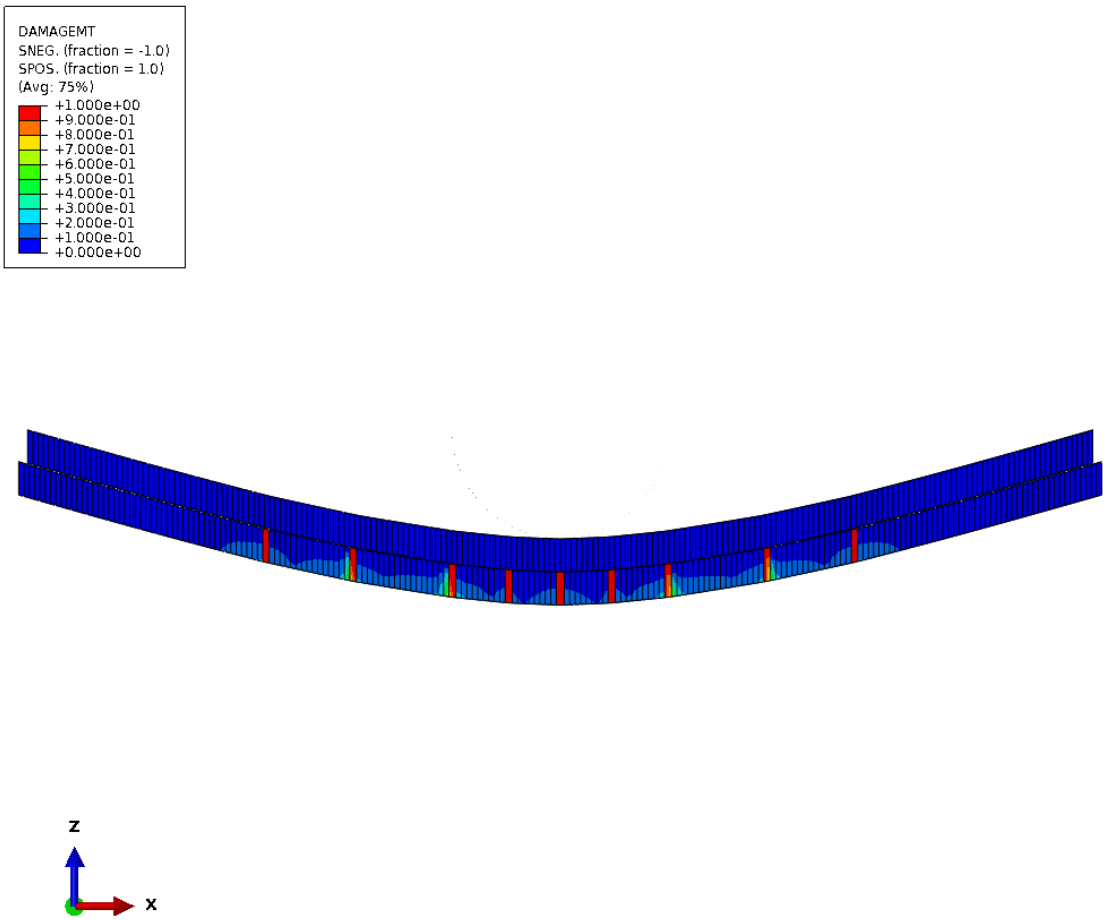

Figure 4.21 – Delamination and matrix tensile damage of the 0/90 beam with two shell layers model with surface-to-surface formulation and the upper layer defined as master (*F* = 1104 N, *w* = 5 mm)

Also, the contact formulation has an influence on the final failure of the structure, with surface-to-surface, in any master/slave configuration, the structure fails (at approximately 20% of the beam length). This is in contrast to node-to-surface formulation, where in any master/slave configuration the structure does not fail at a relatively high displacement. This result was already known from a previous section, but here it can be directly seen on the force displacement plot.

4.2.8. The four shell layers 0/90 model

The purpose of this section is the same as for the previous one, to understand further the influence of "changed" master/slave and the influence of the contact formulations. First is presented the force-displacement graph of the four shell layers model in Figure 4.22.

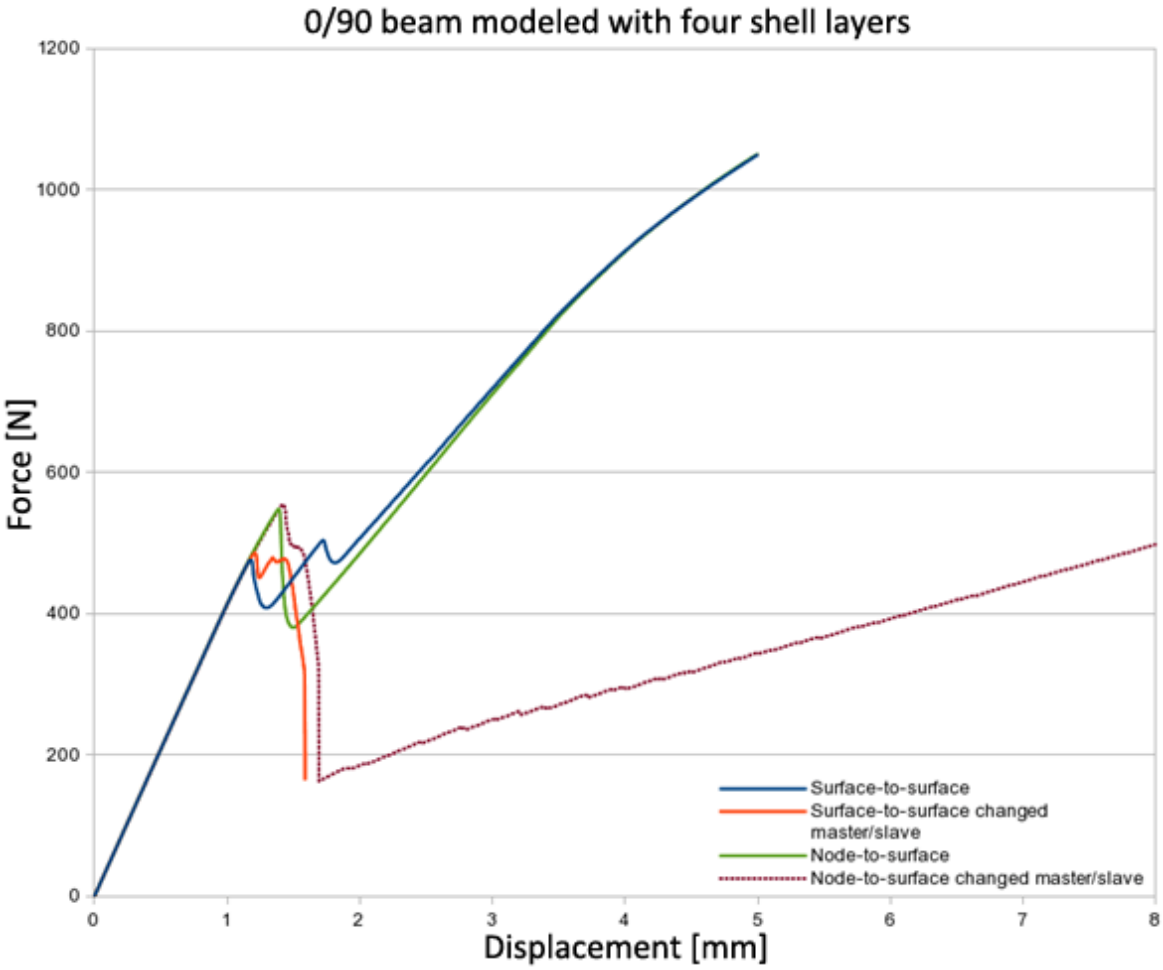

Figure 4.22 – Force-displacement graph for the 0/90 beam with four shell layers

As in the two layers model, changing the master/slave has also a big influence on the curve, but in this case, because of the asymmetric damage evolution on the cohesive surface between the two 0º layers. A second delamination can be observed in this surface, see Figure 4.23. In the force-displacement plot it can be observed for "changed" master/slave a much bigger structural softening after FPF and after the softening the stiffness is much lower. This makes sense, as the failure of the interface between the 0º orientation layers causes additional dissipated fracture energy and stiffness degradation when compared to "normal" master/slave configuration where this interface does not fail.

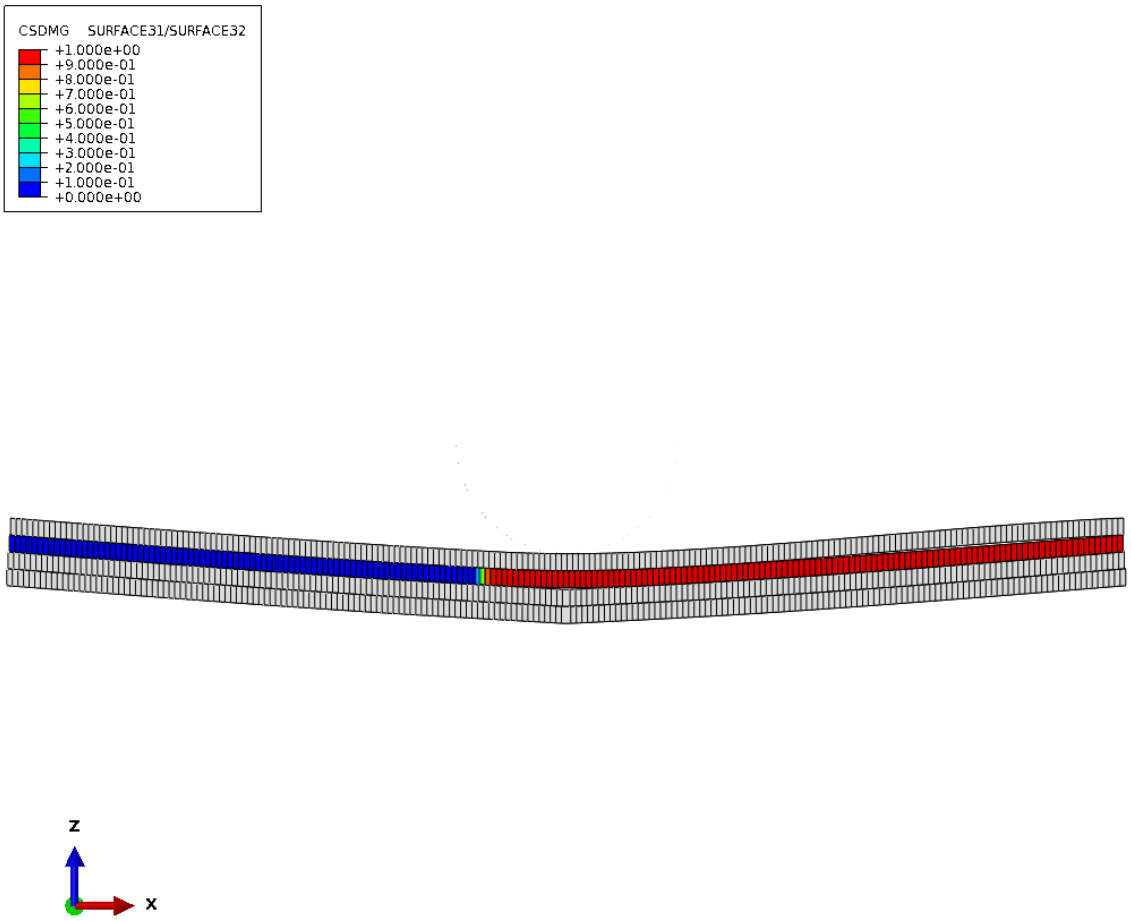

Figure 4.23 – Interface damage of the 0/90 two shell layers model with surface-to-surface formulation and the upper layers defined as master (*F* = 366 N, *w* = 1.55 mm)

As for the contact formulation it influences the strength, as mentioned before, but without a direct comparison in the force-displacement graph, such an observation can be made now. The node-to-surface gives a higher strength when compared to surface-to-surface. Regarding the final failure of the structure, it was stated with the two layers model, that it does not occur with the node-to-surface formulation as it does with the surface-to-surface formulation. This cannot be confirmed with the four layers model, because convergence is limited and does not reach 20% of the beam length (same displacement where the two layers model failed with surface-to-surface formulation).

4.2.9. The eight shell layers 0/90 model

The eight shell layers model is presented in this section. The main difference with this model is that "changed" master/slave configuration, which referred earlier to be a possible flaw in ABAQUS, has particularly no influence in the force-displacement graph, see Figure 4.24. The question remains if by modeling more layers this difference in behavior can be avoided or if this occurs only with the eight shell layers model. This is unknown, because simulations were not made with the twelve layers model in different master/slave surface configuration.

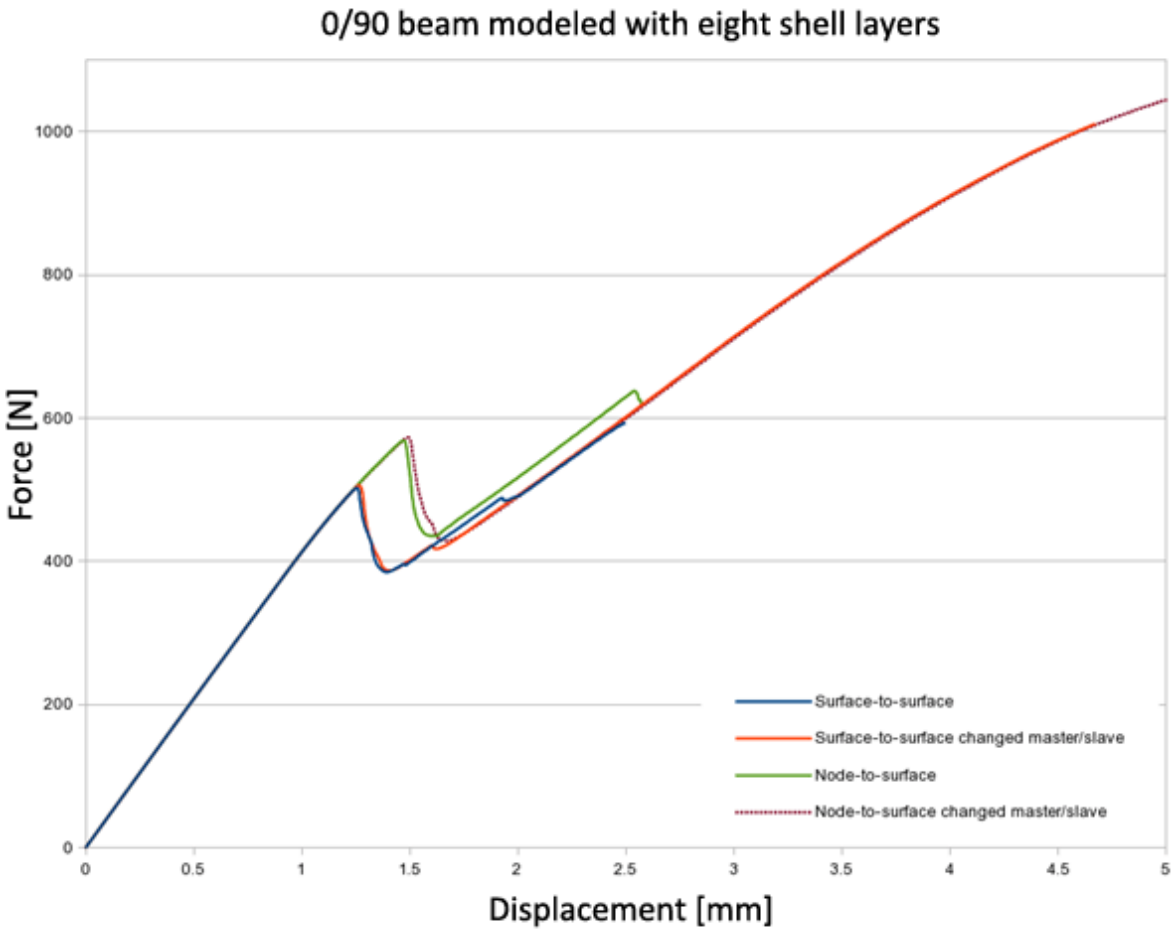

Figure 4.24 – Force-displacement graph for the 0/90 beam with 8 shell layers

As mentioned above for the four shell layers model, the same conclusion can be drawn here, i.e. the models with surface-to-surface contact have a lower strength than the models with node-to-surface contact. As for the final failure of the structure no analysis could be made as convergence is limited.

4.2.7. The eight shell layers $[0/90/0/90]_s$ model

This section presents a model with a different ply layup, previously all models had a 0/90 layup. In this case the model has a symmetric layup (0/90/0/90/90/0/90/0) with eight shell layers and each shell layer represents three plies with a individual thickness of 0.125mm.

Not many results could be obtained with this model, as convergence is limited. FPF could be observed with matrix tensile damage initiation and interface damage near the boundary conditions. The damage on the boundary conditions would already suggest not so credible results, as failure is expected in the center of the beam.

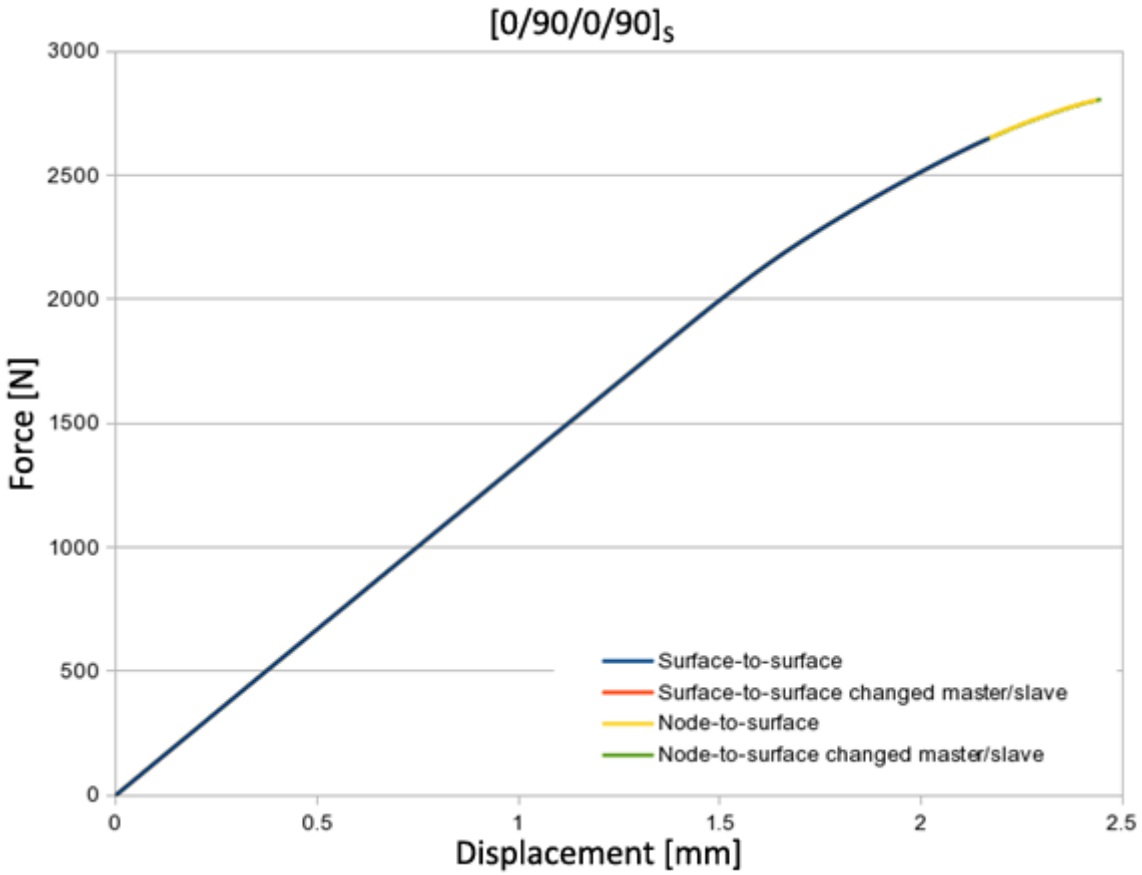

Figure 4.25 – Force-displacement graph for the $[0/90/0/90]_S$ 50mm beam with eight shell layers

The force-displacement graph is represented in Figure 4.25. Non-linear behavior can be observed after damage initiation. In an attempt to obtain further convergence, the stabilization parameters of the ply damage model were increased two times, but without any success. These parameters are related to viscous regularization and increasing them should enhance convergence.

5. Conclusions

The problem for this thesis was to investigate the initial transverse shear stiffness, this was done by using different beam characteristic lengths for the supports and observing the response of the beam. Models were used with a composite section or with two shell layers and an interface, this was necessary to figure out what influence could the interface have over the transverse shear stiffness. In fact, it should have none, but it could be observed that the stiffness is overestimated. This occurred only with conventional shell elements. With continuum shell elements such observations could not be made.

The other topic is related to damage modeling. The strategy adopted was to couple several shell layers together through an interface, allowing the interaction between them. In this topic, it was interesting also to perform numerical simulations not only with conventional shell elements, but also with continuum shell elements, establishing a direct comparison between them. Several problems were encountered with continuum shells, such as "hourglassing", symmetric thickness reduction and no structural softening (as expected).

Because of trouble encountered with continuum shells, it was decided to proceed only with conventional shell elements in the numerical simulations for the preparation of a future experiment. The eight shell layers model that was presented in the thesis provided positive results with a crack growth and delamination in the center of the beam. These results make sense, because the crack growth is where the tensile stresses are maximum according to classical beam theory.

Additional simulations were made to compare different contact formulations. A higher strength could be observed with node-to-surface formulation as with surface-to-surface formulation. The same observation could be made when increasing the number of shell layers to model the specimen. Also, the damage distribution of matrix tensile damage would increase over the length of the ply. Another observation on node-to-surface formulation is that with the two shell layers model final failure of the structure could not be observed at a high displacement (20% of the beam length) as it could be with surface-to-surface contact.

Further simulations were made to figure out what is the influence of changing master/slave definition on the surfaces. It is important to refer that typically this would have no influence or few influences over the results, especially when using surface-to-surface formulation, but in this case there appears to be a flaw in Abaqus. A very different behavior in the two shell layers and four shell layers models could be observed when switching master/slave. With the eight shell layers model this made no difference in the results.

At last, the changed interface values do not have a significant influence over the simulations and provide comparable results.

Bibliography

[1] ABAQUS Manual v6.11. Dassault Systèmes Simulia Corp., Providence, RI, USA (2011)

[2] G. Alfano and M. Crisfield. Finite element interface models for the delamination analysis of laminated composites: mechanical and computational issues.International Journal for Numerical Methods in Engineering, 50:1701-1736 (2001)

[3] M. L. Benzeggagh and M. Kenane. Measurement of Mixed-Mode Delamination Fracture Toughness of Unidirectional Glass/Epoxy Composites with Mixed-Mode Bending Apparatus Comp. Sci and Tech., 56:439-449 (1996)

[4] V. V. Bolotin. Delamination in composite structures: its origin, buckling, growth and stability. Composites Part B, 27B:129-145 (1996)

[5] J. C. Brewer and P. A. Lagace. Quadratic Stress Criterion for initiation of delamination. Journal of Composite Materials, 22:1141-1155 (1988)

[6] P. Camanho, C. Dávila. Progressive damage modeling in fiber-reinforced materials. NASA/TM-2002-211737 (2002)

[7] T. Flatscher, H.E. Pettermann. A constitutive model for fiber-reinforced polymer plies accounting for plasticity and brittle damage including softening - Implementation for implicit FEM. Composite Structures 93:2249 (2011)

[8] A. C. Garg. Delamination - a damage mode in composite structures. Engineering Fracture Mechanics, 29:557-584, (1988)

[9] M. Garnich, V. Akula. Review of Degradation Models for Progressive Failure Analysis of Fiber Reinforced Polymer Composites. Applied Mechanics Reviews 62, 010801 (2009)

[10] Bob Griffiths. Boeing sets pace for composite usage in large civil aircraft. High Performance Composites (May 2005)

[11] Z. Hashin. Failure criteria for unidirectional fiber composites. Journal of Applied Mechanics 47:329-224 (1980)

[12] U. Icardi, S. Locatto and A. Longo. Assessment of Recent Theories for Predicting Failure of Composite Laminates. Applied Mechanics Reviews 60, 76-86 (2007)

[13] Larry Ilcewicz. Lecture notes, Past Experiences and Future Trends for Composite Aircraft Structure, Montana State University Seminar, Bozeman, Montana (October 2009)

[14] R. M. Jones. Mechanics of composite materials. Taylor & Francis Inc., Philadelphia, PA, USA, second edition (1999)

[15] I. Lapczyk and J. A. Hurtado. Progressive damage modeling in fiber reinforced materials. Composites: Part A 38 2333-2341 (2007)

[16] E. R. Lista. Finite Element Simulations of Laminated Composites under Consideration of Nonlinear Ply Material and Delamination. Master Thesis, Vienna University of Technology, Vienna, Austria (2012)

[17] H.E. Pettermann, J. Gager, T. Flatscher: Elasto-plasto-damage modeling of laminated composites. CD-ROM Proceedings of the 6th European Congress on Computational Methods in Applied Sciences and Engineering (ECCOMAS 2012), Vienna, Austria, Eds.: Eberhardsteiner, J.; Böhm, H.J.; Rammerstorfer, F.G., Publisher: Vienna University of Technology, Austria, ISBN: 978-3-9502481-9-7 (September 10-14, 2012)

[18] A. Puck. Festigkeitsanalyse von Faser-Matrix-Laminaten. Carl Hanser Verlag, Munich, Germany (2006)

[19] A. Puck and H. Schürmann. Failure analysis of FRP laminates by means of physically based phenomenological models. Comp. Sci and Tech., 62:1633-1662 (2002)

[20] A. Puck, J. Kopp and M. Knops. Guidelines for the determination of the parameters in Puck's action plane strength criterion. Comp. Sci and Tech., 62:(3) 371-378; (9) 1275 (2002)

[21] P. M. Raman, J. F. Davalos. Static shear correction factor for laminated rectangular beams. Composites Part B 27:285-293 (1996)

[22] F. G. Rammerstorfer and H. J. Böhm. Composite engineering. Lecture notes, Vienna University of Technology, Vienna, Austria (2002)

[23] E. Reissner. The Effect of Transverse Shear Deformation on the Bending of Elastic Plates. J.Appl.Mech. 12, 69-77 (1945)

[24] C. Schuecker, H.E. Pettermann. A continuum damage model for fiber reinforced laminates based on ply failure mechanisms. Composite Structures 76:162-173 (2006)

[25] C. Schuecker, H.E. Pettermann. Constitutive ply damage modeling, FEM implementation, and analyses of laminated structures. Computers and Structures 86:908-918 (2007)

[26] N. G. Stephen. Macaulay's method for a Timoshenko beam. International Journal of Mechanical Engineering Education, 35, (4), 285-292 (2007)

[27] P. B. Stickler. Composite Materials for Commercial Transport - Issues and future research directions. Proceedings of the ASC, 17th Annual Technical Conference, West Lafayette, IN, U.S.A (2002)

[28] http://en.wikipedia.org/wiki/Timoshenko_beam_theory (Retrieved October 2012)

[29] http://en.wikipedia.org/wiki/Euler-Bernoulli_beam_theory (Retrieved October 2012)